Phase Equilibria Modeling of Low-grade Metamorphic Martian Rocks

JGR Planets

RESEARCH ARTICLE
10.1029/2018JE005869

Phase Equilibria Modeling of Low-Grade Metamorphic Martian Rocks

J. Semprich[1], S. P. Schwenzer[2], A. H. Treiman[1], and J. Filiberto[1]

[1]Lunar and Planetary Institute, USRA, Houston, TX, USA, [2]School of Environment, Technology, Engineering and Mathematics, The Open University, Milton Keynes, UK

Key Points:
- Low-grade metamorphic phases detected on Mars can be reproduced by phase equilibria modeling
- Protolith composition and fluid content strongly influence the mineralogy of low-grade metamorphic assemblages
- Warmer geotherms and/or additional heat by hydrothermal or magmatic activity are more favorable for low-grade metamorphic minerals

Supporting Information:
- Supporting Information S1
- Table S1

Correspondence to:
J. Semprich,
jsemprich@lpi.usra.edu

Citation:
Semprich, J., Schwenzer, S. P., Treiman, A. H., & Filiberto, J. (2019). Phase equilibria modeling of low-grade metamorphic Martian rocks. *Journal of Geophysical Research: Planets*, *124*. https://doi.org/10.1029/2018JE005869

Received 30 OCT 2018
Accepted 2 FEB 2019
Accepted article online 6 FEB 2019

Abstract Hydrous phases have been identified to be a significant component of Martian mineralogy. Particularly, prehnite, zeolites, and serpentine are evidence for low-grade metamorphic reactions at elevated temperatures in mafic and ultramafic protoliths. Their presence suggests that at least part of the Martian crust is sufficiently hydrated for low-grade metamorphic reactions to occur. A detailed analysis of changes in mineralogy with variations in fluid content and composition along possible Martian geotherms can contribute to determine the conditions required for subsurface hydrous alteration, fluid availability, and rock properties in the Martian crust. In this study, we use phase equilibria models to explore low-grade metamorphic reactions covering a pressure-temperature range of 0–0.5 GPa and 150–450 °C for several Martian protolith compositions and varying fluid content. Our models replicate the detected low-grade metamorphic/hydrothermal mineral phases like prehnite, chlorite, analcime, unspecified zeolites, and serpentine. Our results also suggest that actinolite should be a part of lower-grade metamorphic assemblages, but actinolite may not be detected in reflectance spectra for several reasons. By gradually increasing the water content in the modeled whole-rock composition, we can estimate the amount of water required to precipitate low-grade metamorphic phases. Mineralogical constraints do not necessarily require an elevated geothermal gradient for the formation of prehnite. However, restricted crater excavation depths even for large impact craters are not likely sampling prehnite along colder gradients, suggesting either a geotherm of ~20 °C/km in the Noachian or an additional heat source such as hydrothermal or magmatic activity.

Plain Language Summary There is evidence that greater amounts of water were present on a younger Mars as compared to the dry conditions observed today. Water not only shapes the surface and forms river beds, deltas, and lakes but also reacts with the existing rocks to form characteristic minerals. Understanding how these minerals formed gives us useful information about how much water may be present in the Martian crust, which is also important for possible habitable environments. Our knowledge about Mars has increased greatly with the data from rovers and orbiters, but we still only have a limited amount of rocks available. Therefore, we use computer models to simulate how rocks from Mars would behave if they were exposed to higher temperatures, pressures, and water. We can estimate how much water is needed to form certain minerals, and that helps us to understand the conditions on Mars over geologic timescales and how and why it is different from Earth.

1. Introduction

Our understanding of Martian mineralogy and geology has improved significantly by extensive data acquisition from imaging spectrometers and in situ investigations from various analytical instruments on the Mars rovers Spirit, Opportunity, and Curiosity. The presence of igneous rocks varying from basaltic to ultramafic compositions is inferred from the widespread occurrence of pyroxenes, olivine, and plagioclase, as observed by visible/near-infrared (VNIR), thermal infrared, and gamma ray spectrometers such as Observatoire pour la Minéralogie, l'Eau, les Glaces, et l'Activité, Compact Reconnaissance Imaging Spectrometer for Mars (CRISM), Thermal Emission Spectrometer, and Gamma Ray Spectrometer (e.g., Bibring et al., 2006; Boynton et al., 2007; Christensen et al., 2001; Murchie et al., 2007), in situ rock analyses on Mars (e.g., Brückner et al., 2003; Gellert et al., 2006; Ming et al., 2008; Schmidt et al., 2014; Squyres et al., 2012; Zipfel et al., 2011), and Martian meteorites of the shergottite, nakhlite, and chassignite group (Bridges & Warren, 2006; Meyer, 2013; Treiman, 2005; Treiman & Filiberto, 2015) and related basaltic meteorites (Agee et al., 2013). In addition, numerous alteration minerals have been identified, including clays,

chlorite, mica, prehnite, epidote, zeolites, serpentine, carbonates, sulfates, hydrated (opaline) silica, oxides, scapolite, and Cl-rich amphibole (e.g., Arvidson et al., 2014; Carter et al., 2013; Changela & Bridges, 2010; Ehlmann et al., 2009; Filiberto et al., 2014; Gendrin et al., 2005; Giesting & Filiberto, 2016; Hicks et al., 2014; Milliken et al., 2008; Murchie et al., 2009; Poulet et al., 2005; Squyres et al., 2008; Treiman, 2005; Vaniman et al., 2014). The presence of hydrous phases indicates multiple diverse aqueous environments and episodes of activity. Most of these hydrous minerals are associated with surface weathering processes, evaporation, diagenesis, and impact-generated hydrothermal systems, as also predicted by thermochemical models (Bridges et al., 2015; Bridges & Schwenzer, 2012; Filiberto & Schwenzer, 2013; Griffith & Shock, 1997; Schwenzer et al., 2016; Schwenzer & Kring, 2013). The occurrence of prehnite, epidote, serpentine, and zeolites, however, is an indication for low-grade metamorphic reactions at deeper levels of Mars' crust.

Although present-day surface conditions on Mars are unfavorable for the permanent presence of liquid water (Carr & Head, 2010), there is geomorphic evidence for at least episodic water activity, particularly during early Mars in the Noachian period (4.1–3.7 Ga), in the form of valley networks, alluvial fans, and lake beds (Fassett & Head, 2008; Harrison & Grimm, 2005; Howard et al., 2005; Irwin et al., 2005). In many of these environments, water was present for an adequate time to alter the mineralogy and precipitate hydrous phases. Studying these minerals, their assemblages, and their geologic context combined with our knowledge about thermodynamics and kinetics of mineral formation in terrestrial systems provides useful information about the conditions of aqueous alteration and low-grade metamorphism such as pressure, temperature, and the composition and amount of fluid (e.g., Ehlmann et al., 2011). By linking the mineralogy to geomorphology, Carter et al. (2013) distinguished several formation processes: (1) surface weathering; (2) detrital deposition, evaporation and formation in fluvial-lacustrine environments; (3) hydrothermal alteration where heat is provided by volcanism, impact cratering (Abramov & Kring, 2005; Filiberto & Schwenzer, 2013; Schwenzer & Kring, 2013), or crustal cooling of early Mars (Parmentier & Zuber, 2007); and (4) diagenesis of sediments and low-grade metamorphism at depth. Although there is no sharp boundary between diagenesis and metamorphism, this study will focus on minerals such as prehnite, epidote, and serpentine, which are commonly categorized as low-grade metamorphic phases on Earth.

While clays are the dominant water-bearing mineral in most of these environments, rocks associated with impact craters seem to be enriched in prehnite and chlorite, which are found mainly in ejecta blankets, crater walls and rims, and central uplifts of fresh craters possibly revealing altered Noachian crust (Carter et al., 2013; Ehlmann et al., 2009, 2011; Loizeau et al., 2012). Prehnite, in particular, is a distinct indicator of alteration at higher temperatures (~150–300 °C), suggesting hydrothermal and/or low-grade metamorphic formation conditions (Ehlmann et al., 2011). Serpentine is formed at similar temperatures but from ultramafic protoliths, while analcime commonly precipitates at lower temperatures (<200 °C) and is an indicator for zeolite-facies metamorphism (Ehlmann et al., 2011; McSween et al., 2015). Epidote, which was only detected in a few locations by remote sensing (Carter et al., 2013), can form at temperatures ≥150 °C. All of these minerals form by prograde metamorphic reactions along geothermal gradients, with temperature and pressure increasing with depth while the porosity and water content of the rocks decrease. However, they may also precipitate due to shorter-lived hydrothermal activity with hotter fluids circulating in the deeper crust, interacting with the preexisting rocks. Impact-induced hydrothermal systems can have life spans of several tens to hundreds of thousand years depending on crater size (Abramov & Kring, 2005) and have been proposed for several craters on Mars (Carrozzo et al., 2017; Mangold et al., 2012; Marzo et al., 2010; Osinski et al., 2013). Although characteristic metamorphic minerals occur in distinct alteration assemblages, for example, prehnite-chlorite-silica (Ehlmann et al., 2011), it cannot be determined by spectral observations from orbit if they are in thermodynamic equilibrium with each other; it is therefore difficult to differentiate hydrothermal alteration from low-grade metamorphism. It has been argued that the detection of hundreds of exposures of prehnite, chlorite, and zeolites specifically in crater ejecta (Carter et al., 2013; Loizeau et al., 2012) cannot be explained by the formation of hydrothermal systems, which mainly affect the center of the crater, and low-grade metamorphic reactions at depth within the Martian crust have been proposed (Carter et al., 2013; Ehlmann et al., 2011). On the other hand, materials in the vicinity of a crater, such as the ejecta blanket, can be affected by aqueous alteration (Schwenzer & Kring, 2013). In contrast to hydrothermal alteration induced by relatively large amounts of water flushing through a rock within a restricted time period in an open system, low-grade metamorphic reactions occur gradually with depth and a relatively limited amount of water approaching a closed system where bulk rock equilibrium is attained.

A number of thermochemical studies predicted the formation of alteration minerals from basaltic and ultramafic protoliths, predominantly in hydrothermal or diagenetic contexts (Bridges & Schwenzer, 2012; Filiberto & Schwenzer, 2013; Griffith & Shock, 1997; Schwenzer et al., 2016; Schwenzer & Kring, 2009, 2013; Zolotov & Mironenko, 2016), but focused on temperatures below 300 °C, relatively high water to rock ratios, and pressures equivalent to less than 10 km in crustal depth. Petrogenetic grids for terrestrial mafic and ultramafic rocks have been used to help recognize low-grade metamorphic assemblages (Ehlmann et al., 2011; Viviano et al., 2013) and for plotting Martian whole-rock compositions (McSween et al., 2015).

Phase diagrams established for terrestrial mafic rocks, however, may not adequately represent Martian basalts, since compositional differences influence mineral stability fields. In addition, petrogenetic grids and A(Al_2O_3), C(CaO), and F(FeO+MgO) diagrams do not address compositional variations as precisely as thermodynamic calculations due to the recalculation of chemical components in ACF projections (e.g., FeO + MgO; no plotting of Na_2O-bearing phases). Furthermore, variations in fluid content can be addressed by thermodynamic modeling, but not with ACF diagrams. We compute phase assemblages for specific whole-rock compositions over a range of pressures and temperatures and use Martian crustal compositions including the shergottite-like Bounce Rock (Zipfel et al., 2011), a basalt from Gusev crater (McSween et al., 2004), two alkaline volcanic rocks (McSween et al., 2006; Stolper et al., 2013), and a poikilitic shergottite that resembles an ultramafic protolith composition (Lodders, 1998). We show that mineral stability fields and proportions are strongly dependent on protolith compositions. By systematically varying the water content, we can predict the formation of hydrous phases along possible Martian geotherms and determine the amount of water required to precipitate the observed low-grade metamorphic minerals. This allows us to estimate how much fluid could be stored in the Martian subsurface, and how this affects subsurface rock properties, and possible habitable environments.

2. Methods

2.1. Model Parameters

All phase diagrams are calculated with the Gibbs free energy minimization software Perple_X 6.8.1 (Connolly, 2005) using an internally consistent thermodynamic data set (Holland & Powell, 1998; 2002 update). The oxides MnO, P_2O_5, and Cr_2O_3 are not considered due to their relatively low abundances and/or an incomplete set of solid solution models defining the compositional space as TiO_2-Na_2O-CaO-K_2O-FeO-MgO-Al_2O_3-SiO_2-H_2O-O_2 (TiNCKFMASHO). The sum of all considered oxides is normalized to 100% by Perple_X at every pressure-temperature condition. We compute sections of a phase diagram for a specified starting composition, so-called pseudosections, in the range of 0–0.5 GPa and 150–450 °C. Fluid is treated as pure H_2O, which is justified by the fact that CO_2 is a negligible fluid component at temperatures below 400 °C at least in terrestrial environments (e.g., Massonne, 2010; Willner et al., 2013), and we consider subsurface conditions where the fluids are not in contact with the Martian atmosphere. We use the Compensated-Redlich-Kwong equation of state (Holland & Powell, 1998). In Perple_X, all properties of water are obtained by the specified equation of state and therefore vary with conditions. The amount of Fe^{3+} in Perple_X is represented by the O_2 content, which was chosen at values between 0.12 and 0.15 to account for phases with Fe^{3+} end-members such as epidote, clinopyroxene, and pumpellyite. While this is a fixed value, and not a buffer, it represents the oxygen fugacity of the system at conditions similar to a quartz-fayalite-magnetite (QFM) buffer. Table 1 lists all solid solution models, ideal solutions, and pure phases selected for our phase equilibria calculations. Vesuvianite, andradite, grossular, and Na-phlogopite were excluded due to their calculated stabilities exceeding their stabilities in naturally occurring rocks, and they have not been detected on Mars. To simplify the phase diagrams, we also excluded riebeckite, zoisite, and anthophyllite since they are only stable at conditions not relevant for low-grade metamorphism on Mars.

2.2. Input Parameters

2.2.1. Protolith Compositions

In a first step, we calculate pseudosections for water-saturated conditions using the compositions of an average mid-ocean ridge basalt (MORB; Gale et al., 2013) and Bounce Rock (Zipfel et al., 2011) to represent a basaltic shergottite (Table 2). The MORB composition allows an assessment of our model with respect to

Table 1
List of Minerals Used in Phase Equilibria Calculations Including Independent End-Members of Solid Solutions, Their Abbreviations as They Appear on All Figures, and References for Solid Solution Models (Except for Pure Minerals and Ideal Solutions)

Mineral or solid solution, abbreviation used in Perple_X	Formula of end-members	Abbreviation	Reference
Amphiboles			
Actinolite, Act(M)	*tremolite:* $Ca_2Mg_5Si_8O_{22}(OH)_2$ *actinolite:* $Ca_2Mg_3Fe_2Si_8O_{22}(OH)_2$ *glaucophane:* $Na_2Mg_3Al_2Si_8O_{22}(OH)_2$ *magnesioriebeckite:* $Na_2Mg_3Fe_2Si_8O_{22}(OH)_2$	Act	Massonne and Willner (2008)
Clinoamphibole, GlTrTsPg	*tremolite:* $Ca_2Mg_5Si_8O_{22}(OH)_2$ *Fe-tremolite:* $Ca_2Fe_5Si_8O_{22}(OH)_2$ *pargasite:* $NaCa_2Mg_4Al_3Si_6O_{22}(OH)_2$ *tschermakite:* $Ca_2Mg_3Al_4Si_6O_{22}(OH)_2$ *glaucophane:* $Na_2Mg_3Al_2Si_8O_{22}(OH)_2$	Amp	Wei and Powell (2003) and White et al. (2003)
Pyroxenes			
Clinopyroxene, Cpx (HP)	*diopside:* $CaMgSi_2O_6$ *hedenbergite:* $CaFeSi_2O_6$ *jadeite:* $NaAlSi_2O_6$ *Ca-tschermaks:* $CaAl_2SiO_6$ *acmite:* $NaFeSi_2O_6$	Cpx	Holland and Powell (1996, 1998)
Orthopyroxene, Opx (HP)	*enstatite:* $Mg_2Si_2O_6$ *ferrosilite:* $Fe_2Si_2O_6$ *Mg-tschermaks:* $MgAl_2SiO_6$	Opx	Holland and Powell (1996, 1998)
Feldspar			
K-feldspar, Kf	*microcline:* $KAlSi_3O_8$ *albite:* $NaAlSi_3O_8$	Ab[a]	Thompson and Waldbaum (1969)
Plagioclase, Pl(h)	*high-albite:* $NaAlSi_3O_8$ *anorthite:* $CaAl_2Si_2O_8$	Pl	Newton et al. (1980)
Phyllosilicates			
Chlorite, Chl(W)	*clinochlore:* $Mg_5Al_2Si_3O_{10}(OH)_8$ *daphnite:* $Fe_5Al_2Si_3O_{10}(OH)_8$ *amesite:* $Mg_4Al_4Si_2O_{10}(OH)_8$ *Al-free-chlorite:* $Mg_6Si_4O_{10}(OH)_8$	Chl	White et al. (2014)
Biotite, Bio (TCC)	*annite:* $KFe_3AlSi_3O_{10}(OH)_2$ *phlogopite:*	Bt	Tajčmanová et al. (2009)

Table 1 *(continued)*

Mineral or solid solution, abbreviation used in Perple_X	Formula of end-members	Abbreviation	Reference
	$KMg_3AlSi_3O_{10}(OH)_2$ *eastonite:* $KMg_2Al_3Si_2O_{10}(OH)_2$		
White mica, Mica (M)	*margarite:* $CaAl_4Si_2O_{10}(OH)_2$ *muscovite:* $KAl_3Si_3O_{10}(OH)_2$ *paragonite:* $NaAl_3Si_3O_{10}(OH)_2$	Ms	Massonne and Willner (2008)
Stilpnomelane, Stp(M)	*stilpnomelane:* $K_5Al_5Fe_{48}Si_{67}O_{168}(OH)_{48}\cdot 36H_2O$ *magnesio-stilpnomelane:* $K_5Al_5Mg_{48}Si_{67}O_{168}(OH)_{48}\cdot 36H_2O$	Stp	Massonne and Willner (2008)
Serpentine, Atg (PN)	*antigorite:* $Mg_{48}Si_{34}O_{85}(OH)_{62}$ *Fe-antigorite:* $Fe_{48}Si_{34}O_{85}(OH)_{62}$	Atg	Padrón-Navarta et al. (2013)
Talc, T	*talc:* $Mg_3Si_4O_{10}(OH)_2$ *Fe-talc:* $Fe_3Si_4O_{10}(OH)_2$ *talc-tschermaks:* $Mg_2Al_2Si_3O_{10}(OH)_2$	Tlc	ideal
Zeolites			
analcime	$NaAlSi_2O_6\cdot H_2O$	anl	pure
laumontite	$CaAl_2Si_4O_{12}\cdot 4H_2O$	lmt	pure
stilbite	$CaAl_2Si_7O_{18}\cdot 7H_2O$	stb	pure
wairakite	$CaAl_2Si_4O_{12}\cdot 2H_2O$	wrk	pure
Other silicates			
prehnite	$Ca_2Al_2Si_3O_{10}(OH)_2$		pure
Pumpellyite, Pu(M)	*pumpellyite:* $Ca_4MgAl_5Si_6O_{21}(OH)_7$ *ferro-pumpellyite:* $Ca_4FeAl_5Si_6O_{21}(OH)_7$ *ferri-pumpellyite:* $Ca_4MgFe_5Si_6O_{21}(OH)_7$	Pmp	Massonne and Willner (2008)
Epidote, Ep (HP11)	*Fe-epidote:* $Ca_2Fe_2AlSi_3O_{12}(OH)$ *clinozoisite:* $Ca_2Al_3Si_3O_{12}(OH)$	Ep	Holland and Powell (2011)
Olivine, O (HP)	*forsterite:* Mg_2SiO_4 *fayalite:* Fe_2SiO_4	Ol	Holland and Powell (1996, 1998)
Spinel, Sp (WPC)	*spinel:* $MgAl_2O_4$ *hercynite:* $FeAl_2O_4$ *ulvöspinel:* Fe_2TiO_4 *magnetite:* Fe_3O_4	Sp	White et al. (2003)
titanite (sphene)	$CaTiSiO_5$	ttn	pure
quartz	SiO_2	qz	pure
lawsonite	$CaAl_2Si_2O_7(OH)_2\cdot H_2O$	lws	pure
nepheline	$NaAlSiO_4$	nph	pure
Oxides/Hydroxides			
Ilmenite, IlGy	*ilmenite:* $FeTiO_3$ *geikielite:*	Ilm	ideal

Table 1 *(continued)*

Mineral or solid solution, abbreviation used in Perple_X	Formula of end-members	Abbreviation	Reference
	$MgTiO_3$		
magnetite	Fe_3O_4	mag	pure
Brucite, B	*brucite:* $Mg(OH)_2$ *Fe-brucite:* $Fe(OH)_2$	Brc	ideal

[a]In our computed phase equilibria diagrams, Kf is predominantly albite; therefore, we use Ab as abbreviation.

previous studies of low-grade metamorphic metabasic rocks (e.g., Massonne & Willner, 2008; Willner et al., 2013). Using the composition of Bounce Rock enables us to compare mineral stability fields of terrestrial and Martian basalts.

Bounce Rock, which was analyzed by the Alpha Particle X-ray Spectrometer (APXS) on the Mars Exploration Rover (MER) Opportunity on Meridiani Planum, shows textural, mineralogical, and chemical properties similar to basaltic shergottites (Zipfel et al., 2011) and is therefore considered a reasonable representative for a Martian basaltic composition. To ensure the lowest amount of soil/dust contamination, we use the bulk chemistry measurement of Case, the abraded target on Bounce Rock (Zipfel et al., 2011). The analyzed composition of Bounce Rock has significantly less Al_2O_3 and Na_2O and more FeO and CaO than the MORB (Table 2).

In addition to a shergottite basalt (Bounce Rock), we study representatives of the compositional range of reported igneous compositions from Mars varying from olivine-rich basalts to alkali-enriched mugearite, and a silica-poor cumulate. Since most of these compositions were analyzed at different locations, they reflect possible regional geological differences on Mars, which influence the formation and stability of low-grade metamorphic phases. All in situ measurements are bulk rock estimates from APXS analyses taken from a variety of surfaces ranging from abraded, to Rock Abrasion Tool (RAT) brushed, to *as is*. Consequently, the reported analyses contain various amounts of Martian dust, which is basaltic with high S and Cl and therefore most influences compositions that differ from the Martian average (Schmidt et al., 2018). Nevertheless, we use the reported compositions without corrections for dust because (1) a comparison to previous results (e.g., McSween et al., 2015) is consistent, (2) the bulk composition is merely a starting

Table 2
Whole-Rock Compositions and Bulk Rock Estimates From APXS Analyses for Mid-Ocean Ridge Basalt and Martian Protoliths Used in Our Calculations

	N-MORB[a]	Bounce Rock[b]	Humphrey[c]	Backstay[d]	Jake_M[e]	ALH A77005[f]
SiO_2	50.42	51.6	46.1	49.6	51.3	42.2
TiO_2	1.53	0.74	0.52	0.93	0.65	0.39
Al_2O_3	15.13	10.5	10.6	13.3	15.7	2.9
FeO[g]	9.81	14.4	17.9	13.7	10.8	20.1
MgO	7.76	6.8	12.2	8.32	4.4	28.2
CaO	11.35	12.1	7.7	6.05	6.7	3.2
Na_2O	2.83	1.7	2.59	4.16	7.0	0.47
K_2O	0.14	0.1	0.06	1.07	2.17	-

Note. Bounce Rock represents a basaltic shergottite, Humphrey an olivine-rich basalt, Backstay a mildly alkaline basalt, and Jake_M a Martian mugearite. ALH A77005 is a poikilitic shergottite resembling an ultramafic composition. FeO is the total iron in the composition. The sum is normalized by Perple_X taking into account the variable water content in the modeled phase diagrams.
[a]Gale et al. (2013). [b]APXS analysis by MER Opportunity (e.g., Zipfel et al., 2011). [c]Extrapolated from APXS analyses by MER Spirit (e.g., McSween et al., 2004). [d]APXS analysis by MER Spirit (e.g., McSween et al., 2006). [e]APXS analysis by MSL Curiosity (e.g., Stolper et al., 2013). [f]Lodders (1998). [g]Total iron.

point and all oxides vary significantly more with water content and metamorphic conditions compared to differences that result from dust contribution to the initial composition, and (3) certain components such as Cl and S are currently not considered in our calculations.

Humphrey is the least altered example of Adirondak class basalts, as analyzed after being RAT abraded by APXS on Spirit at Gusev Crater (McSween et al., 2004). It is an olivine-rich picritic basalt containing up to 25% megacrystic olivine (McSween et al., 2004). Experimental results suggest that the Adirondak class basalts represent fractionated magmas (Filiberto et al., 2008). Compositionally, Humphrey has significantly higher FeO and MgO compared to Bounce Rock and lower SiO_2 and CaO (Table 2). Also, it contains more Na_2O than Bounce Rock but less than MORB.

Backstay is a trachybasalt (i.e., hawaiite) from the Columbia Hills in Gusev crater; texturally, it is aphanitic and has been interpreted to represent lava or a dike rock (McSween et al., 2006). The APXS analysis was obtained by Spirit after a RAT surface brushing. Its SiO_2 and MgO contents are between those of Bounce Rock and Humphrey, but it has higher Al_2O_3 than either and even lower CaO than Humphrey (Table 2). It also shows significantly higher amounts of Na_2O and K_2O than Bounce Rock, Humphrey, and MORB.

Jake_M, the first rock analyzed by the Curiosity rover in Gale crater, is compositionally distinct from all other Martian igneous rocks but similar to terrestrial mugearites, which form in ocean island and rift settings (Stolper et al., 2013). We use the average APXS composition given by Stolper et al. (2013), which has been obtained at the surface without any dust removal. Jake_M has SiO_2, Al_2O_3, and FeO contents similar to MORB but lower MgO and CaO and significantly higher Na_2O and K_2O.

The poikilitic shergottite ALH A77005 (Lodders, 1998) was chosen because it is a representative Martian ultramafic rock: silica-undersaturated, Al-poor but FeO and MgO-rich, with low CaO and alkalis (Table 2).

2.2.2. Water Content

Based on gamma ray spectrometry, the Mars surface layer in the low-latitude and midlatitude regions of Mars contains hydrogen equivalent to 1.5%–7.5% H_2O (Boynton et al., 2007). While these reflect surface or near-surface values of present-day Mars, and the water content in earlier time periods and the deeper subsurface is not known, we see this range as a valid starting point and adopt similar values for our calculations. Curiosity's Dynamic Albedo of Neutron (DAN) instrument yields mean estimates of the water equivalent of hydrogen between 1.5–1.7 wt % for the top layer (10–20 cm) and 2.2 to 3.3 wt % for the bottom layer with water content being as high as ~5 wt % locally along the rover's traverse in Gale crater (Mitrofanov et al., 2014). These values are for sediments in a region where low-grade metamorphic phases have not been reported by VNIR spectra but also give an estimate of water availability. There is evidence that clay minerals have been uplifted in impact crater central peaks from depths of at least 7 km, and possibly even deeper (Flahaut et al., 2012; Mustard et al., 2008; Sun & Milliken, 2015), suggesting that the water contents obtained by DAN can be extrapolated to these depths. Our aim is to study the changes in mineralogy ranging from very low water content up to water saturation, which is why we have chosen to vary the amount of water from 0 to 6 wt %. Our modeled protolith compositions are water saturated between 5 and 6 wt % H_2O, except for the cumulate (7–8 wt %).

2.2.3. Geotherms and Pressure-to-Depth Conversion

Radiogenic heat production in Mars was likely much greater in the Noachian period, which would have caused a higher global geothermal gradient. However, estimating thermal gradients for specific locations is complicated by changes in radiogenic heat production in various geologic provinces (McSween et al., 2015). Heat flow estimates in the Noachian epoch range from >35 to 60 mW/m^2, which correspond to thermal gradients between >14 °C/km and 20 °C/km (McGovern et al., 2004). McSween et al. (2015) calculate a Noachian geotherm of 12 °C/km for the Nili Fossae region, where many of the low-grade metamorphic phases have been reported. Based on these estimates, we choose geotherms of 10 °C/km, 13 °C/km, and 20 °C/km, along which we calculate low-grade metamorphic equilibrium assemblages at varying water contents.

Depths below the surface are calculated from the lithostatic pressure via the formula $P = \rho g h$; for Mars, we use a mean crustal density of 2,960 kg/m^3 (Turcotte et al., 2002) and g of 3.727 m/s^2; for Earth, we use 3,200 kg/m^3 and 9.8 m/s^2.

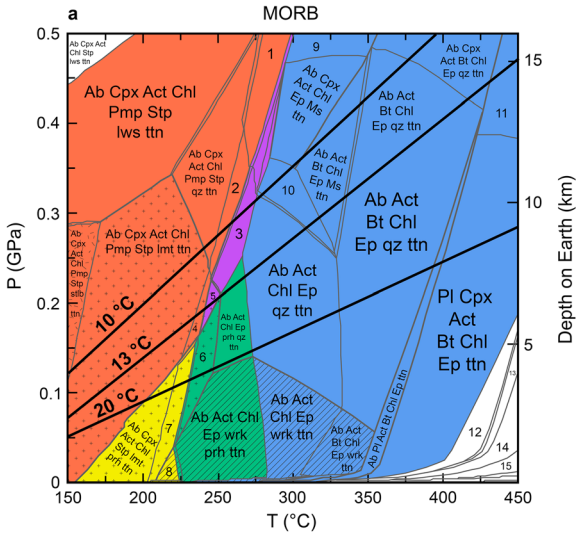

1: Ab Cpx Act Chl Ms Pmp qz ttn; 2: Ab Cpx Act Chl Pmp qz ttn; 3: Ab Act Chl Ep Pmp qz ttn; 4: Ab Cpx Act Chl Pmp lmt ttn; 5: Ab Act Chl Ep Pmp lmt ttn; 6: Ab Act Chl Ep lmt prh ttn; 7: Ab Cpx Act Chl lmt prh ttn; 8: Ab Cpx Act Chl wrk prh ttn; 9: Ab Cpx Act Chl Ep Ms qz ttn; 10: Ab Act Chl Ep Ms ttn; 11: Pl Cpx Act Bt Ep qz ttn; 12 Pl Cpx Act Bt Chl ttn mag; 13: Pl Cpx Act Bt Chl ttn ilm; 14: Pl Cpx Act Bt Chl ttn ilm mag; 15: Pl Cpx Act Bt Chl ilm mag

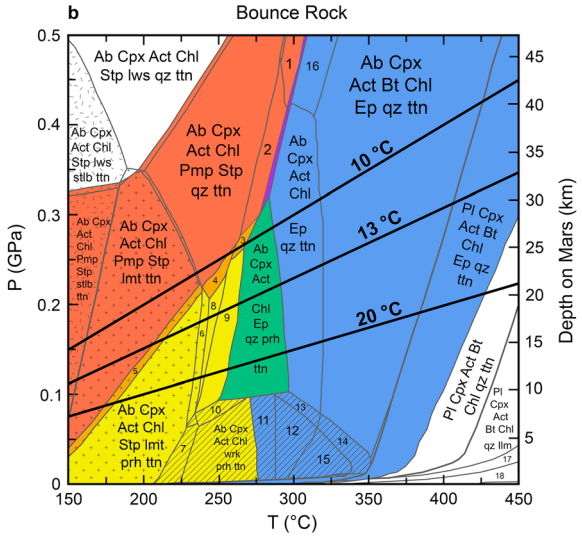

1: Ab Cpx Act Chl Ms Pmp qz ttn; 2: Ab Cpx Act Chl Pmp qz ttn; 3: Ab Cpx Act Chl Pmp prh qz ttn; 4: Ab Cpx Act Chl Pmp Stp prh qz ttn; 5: Ab Cpx Act Chl Pmp Stp lmt prh ttn; 6: Ab Cpx Act Chl Stp lmt prh qz ttn; 7: Ab Cpx Act Chl Stp wrk prh qz ttn; 8: Ab Cpx Act Chl Stp prh qz ttn; 9: Ab Cpx Act Chl prh qz ttn; 10: Ab Cpx Act Chl prh wrk qz ttn; 11: Ab Cpx Act Chl Ep wrk qz ttn; 12: Ab Cpx Act Chl Ep wrk ttn; 13: Ab Cpx Act Chl Ep wrk qz ttn; 14: Ab Cpx Act Bt Chl Ep wrk qz ttn;15: Ab Cpx Act Bt Chl Ep wrk ttn; 16: Ab Cpx Act Chl Ep Ms qz ttn; 17: Pl Cpx Act Bt Chl qz ilm mag; 18: Pl Cpx Ol Act Bt qz ilm mag.

Figure 1. Pseudosections showing stable phases of water-saturated compositions of (a) MORB and (b) Bounce Rock, measured by MER Spirit and equivalent to a basaltic shergottite. Table 1 provides a list of all solid solution models and abbreviations used in our models and figures, while whole-rock compositions are listed in Table 2. Very small phase fields are shown only as a bold line and are not labeled. The depth scale for Earth and Mars is calculated using the formula $P = \rho g h$ using a mean crustal density of 2,960 kg/m^3 and g of 3.727 m/s^2 for Mars and 3,200 kg/m^3 and 9.8 m/s^2 for Earth. Possible geotherms of 10 °C/km, 13 °C/km, and 20 °C/km are represented by the bold black lines. Colors represent fields with the following phases: pumpellyite, red; pumpellyite and epidote, purple; epidote, blue; prehnite, yellow; prehnite and epidote, green; and prehnite and pumpellyite, orange. Zeolites are represented by the following textures: stilbite, hatched; laumontite, crosses; and wairakite, diagonal lines.

3. Results

3.1. Phase Relations

Figure 1 shows pseudosections for the MORB and Bounce Rock compositions (Table 2), calculated for water saturation at *P-T* conditions of 0–0.5 GPa and 150–450 °C. Solid solutions selected for all phase equilibria calculations are given in Table 1. The phase fields for our MORB composition (Figure 1a) are similar to the pseudosections for low-grade metabasic rocks presented by Massonne and Willner (2008) and Willner et al. (2013). Chlorite and Ca-rich amphibole (actinolite) are stable over the whole *P-T* range. Feldspar is the main Na-bearing phase and dominated by albite component (≥95%) but increases in anorthite with higher temperatures. Clinopyroxene is a solid solution of hedenbergite and diopside with lesser proportions of acmite and is present over a large *P-T* range, except for temperatures between 280 °C and 350 °C and pressures less than 0.3 GPa. Pumpellyite and stilpnomelane are restricted to temperatures below 250 °C–300 °C, over most of the pressure range. At temperatures above 300 °C, biotite is the dominant potassium-bearing hydrous phase (but restricted to <1 vol % due to low K_2O in the composition), while muscovite is only present at a limited range of ~270–350 °C above 0.3 GPa. Prehnite is stable at pressures <0.25 GPa and temperatures <280 °C. There is a very limited field of coexistence of pumpellyite and prehnite, as noted previously for Earth rocks, leading to the suggestion that the mineral pair should not be used to represent a metamorphic facies (Frey et al., 1991; Willner et al., 2013). Zeolites are present in the lower temperature and pressure region, transitioning from stilbite to laumontite to wairakite with increasing temperature. Epidote forms at temperatures above 225 °C and is stable over a large portion of the phase diagram but disappears at 400 °C (at $P \leq 0.15$ GPa). Lawsonite is stable at pressures above 0.3 GPa at relatively low temperatures (≤280 °C). The predominant Ti-bearing phase is titanite, which is replaced by ilmenite at higher temperatures (~400 °C).

Although the composition of Bounce Rock yields metamorphic mineral assemblages (Figure 1b) similar to those of MORB, their mineral proportions differ significantly. Actinolite, chlorite, and feldspar (albite) are present for both compositions over the whole *P-T* range; the pumpellyite field is reduced at higher pressures but expands with increasing temperatures (Figures 1b and 2a). Prehnite stability is increased toward slightly higher pressures and higher temperatures. As a result, there is more overlap of the pumpellyite and prehnite phase fields than in the MORB composition (Figure 1). Clinopyroxene is present over the whole *P-T* range. Zeolites show variations in their phase stability fields. Epidote is precipitated at slightly higher temperatures and absent at lower temperatures (Figure 2b). The lawsonite and mica fields are reduced compared to the MORB composition. Stilpnomelane is the low-*T* potassium-bearing hydrous phase and is replaced by biotite at higher pressures. As in the MORB composition, titanite is the predominant Ti-bearing phase, only replaced by ilmenite at high-*T* and low-*P*.

The metamorphic mineral assemblages of the Humphrey composition (phase diagram in supplementary materials) are dominated by chlorite, clinopyroxene, albite, and actinolite. Prehnite and epidote are absent, while the pumpellyite stability field is restricted to pressures above 0.4 GPa. Analcime is the stable zeolite instead of more Ca-bearing zeolites.

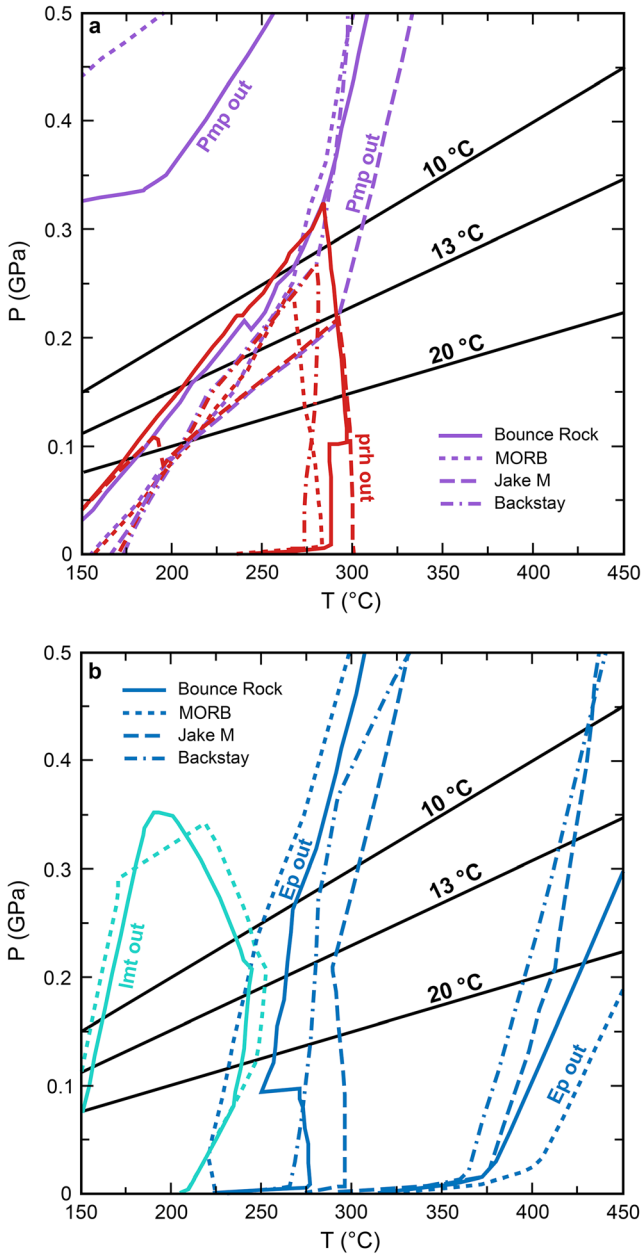

Figure 2. Variations of phase stability fields with protolith compositions for (a) prehnite and pumpellyite and (b) laumontite and epidote. The prehnite field is largest in Bounce Rock, which also results in a smaller pumpellyite field. Laumontite is only present in MORB and Bounce Rock, while the other compositions either have analcime or no zeolites. The bold black lines represent geotherms at 10 °C/km, 13 °C/km, and 20 °C/km.

The mineral assemblages of the Jake_M composition (phase diagram in supporting information) contain clinopyroxene, albite, chlorite, and analcime over most of the *P-T* range. Actinolite and other zeolites are absent. The pumpellyite field is extended to both higher temperatures and pressures compared to both MORB and Bounce rock, which causes reduced prehnite stability (Figure 2a). Epidote precipitates at higher temperatures (~300 °C) compared to Bounce Rock and MORB, and the Epidote-out reaction occurs at lower temperatures. Due to the higher potassium content in the whole-rock composition, biotite is more abundant (14–20 vol %) and is present over a large *P-T* range.

Most phase fields for the Backstay composition (phase diagram in the supporting information) are dominated by albite, chlorite, and clinopyroxene. The only stable zeolite is analcime, which is present at lower temperatures. The pumpellyite and prehnite fields are comparable to those for MORB (see also Figure 2a). Actinolite is a stable phase mostly outside of the pumpellyite stability field. Epidote is precipitated at 270 °C–300 °C and disappears at ~370 °C–470 °C. Biotite (up to 10 vol %) replaces stilpnomelane at temperatures above 200 °C.

The alteration mineralogy of the poikilitic shergottite (phase diagram in the supporting information) is dominated by serpentine (antigorite), olivine, and clinopyroxene, with minor amounts of chlorite, spinel, and ilmenite. Small proportions of brucite (~2 vol %) are present at temperatures up to ~350 °C.

3.2. Compositional Variations in the Modeled Phase Diagrams

In the following section we will discuss how compositional differences in the protolith influence modeled mineral stability fields with the main focus on low-grade metamorphic minerals detected on Mars. Neither prehnite nor pumpellyite are stable phases along realistic geotherms for basaltic compositions such as Humphrey at water-saturated conditions and within the *P-T* space considered. We attribute this to the high percentages of FeO and MgO in the protolith, causing the formation of large amounts (~40 vol %) of chlorite, which consumes Al_2O_3 but not CaO. This results in the presence of significant amounts of clinopyroxene with higher portions of CaO (~22–26 wt %) compared to actinolite (~12 wt %), thereby destabilizing other Ca-bearing mineral phases. The pumpellyite-prehnite pair forms in all other mafic compositions but shows variations in their stability fields (Figure 2a). Compositions with a combination of high Al_2O_3 (13–15 wt %) and low CaO (6–7 wt %), such as Jake_M and Backstay, are favorable for a large pumpellyite stability field at the expense of prehnite. The Bounce Rock composition, on the other hand, with high CaO (> 12 wt %) and lower Al_2O_3 (10.5 wt %) yields the largest prehnite stability field. Higher CaO, as in Bounce Rock, results in a larger stability field for epidote, while the compositions of Jake_M and Backstay yield reduced epidote stability both in the lower- and higher-temperature regions (Figure 2b). Compositions with CaO contents lower than ~8 wt % but Na_2O higher than 2.5 wt % (Humphrey, Jake_M, and Backstay) are favorable for the formation of the sodic zeolite analcime instead of the more Ca-rich zeolites stilbite, laumontite, and wairakite.

3.3. Effect of Water Content on Formation of Hydrous Phases

In order to explore how changes in volatile content influence the modeled mineralogy, we vary the water content of the system from 0 to 6 wt % along specific geotherms of 10 °C/km, 13 °C/km, and 20 °C/km (Figure 1b). An example is shown in Figure 3 for the Bounce Rock composition and a 13 °C/km

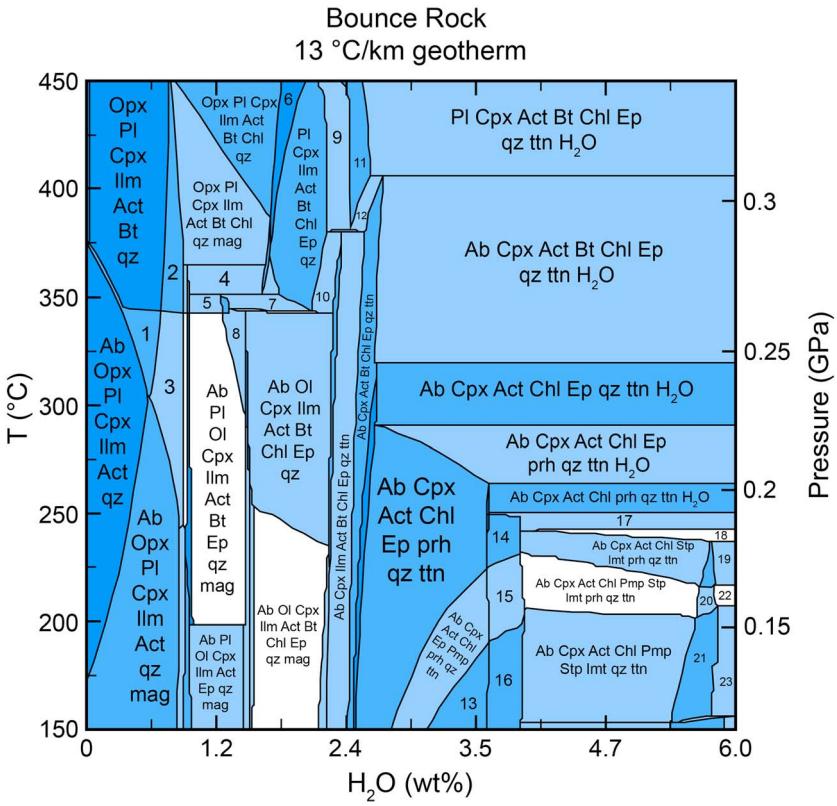

1: Ab Opx Pl Cpx Ilm Act Bt qz; 2: Opx Pl Cpx Ilm Act Bt qz mag; 3: Opx Pl Cpx Ilm Act Bt qz mag; 4: Pl Cpx Ol Ilm Act Bt Chl qz mag; 5: Pl Cpx Ol Ilm Act Bt Ep qz mag; 6: Pl Cpx Ilm Act Bt Chl qz; 7: Pl Ol Cpx Ilm Act Bt Chl Ep qz; 8: Ab Pl Ol Cpx Ilm Act Bt Ep qz; 9: Pl Cpx Ilm Act Bt Chl Ep ttn qz; 10: Ab Pl Cpx Ilm Act Bt Chl Ep qz; 11: Pl Cpx Act Bt Chl Ep qz ttn; 12: Ab Pl Cpx Act Bt Chl Ep qz ttn; 13: Ab Cpx Act Chl Ep Pmp qz ttn; 14: Ab Cpx Act Chl Stp prh qz ttn; 15: Ab Cpx Act Chl Pmp Stp prh qz ttn; 16: Ab Cpx Act Chl Pmp Stp qz ttn; 17: Ab Cpx Act Chl Stp prh q ttn H_2O; 18: Ab Cpx Act Chl Stp prh lmt qz ttn H_2O; 19: Ab Cpx Act Chl Stp lmt prh ttn H_2O; 20: Ab Cpx Act Chl Pmp Stp prh lmt sph; 21: Ab Cpx Act Chl Pmp Stp lmt ttn; 22: Ab Cpx Act Chl Pmp Stp lmt prh ttn H_2O; 23: Ab Cpx Act Chl Pmp Stp lmt ttn H_2O

Figure 3. Phase fields along a 13 °C/km geotherm (see Figure 1b) for the composition of Bounce Rock with varying water content from 0 to 6 wt%. Colors represent the degree of variance ranging from 8 phases (darker blue) to 10 phases (white).

geotherm. To better compare when hydrous phases appear in the protoliths, we have chosen a point on the 13 °C/km geotherm at 200 °C and a corresponding pressure of ~0.15 GPa.

In the Bounce Rock composition, the smallest amount of water results in the formation of actinolite. Biotite and epidote precipitate at ~1 wt % water, respectively. At higher values of 1.5 wt % H_2O, the first chlorite appears. Prehnite formation requires ~2.5 wt % H_2O in the system, while pumpellyite requires 3.2 wt %. Laumontite forms at water contents as high as ~4 wt %. For some minerals, these values vary significantly along the geotherm (see Figure 3). At higher *P-T*, for example, biotite forms at less than 1 wt % H_2O, and chlorite is precipitated at <1.5 wt %. Pumpellyite also requires less water at temperatures lower than 200 °C. In the Humphrey composition, actinolite and biotite are present at very low water content. The first chlorite forms at ~1.2 wt % H_2O, while analcime requires ~5.2 wt %. In the composition of Jake_M, biotite is present at very low water content, while epidote precipitates at 0.8 wt %. Chlorite and pumpellyite require 0.9 and 1.3 wt %, and analcime forms at 1.6 wt % H_2O. In the Backstay composition, biotite is stable at very low water content, while actinolite forms at 0.4 wt %. Chlorite, epidote, and pumpellyite require 1.2, 1.9, and 3.7 wt %, respectively. Prehnite and analcime are not present at conditions of 200 °C, 0.15 GPa, and a 13 °C/km geotherm. In cumulate ALH A77005 composition, amphiboles (predominantly tremolite) precipitate at very low water contents, while chlorite and antigorite form at 0.5 and 2.7 wt%, respectively. Talc forms at ~0.9 wt % H_2O but is not stable above 4.7 wt % H_2O.

In summary, actinolite (and tremolite in the cumulate), chlorite, biotite, and epidote require relatively low water contents in the whole-rock compositions and are the first hydrous phases to precipitate. The formation of prehnite and pumpellyite depends strongly on composition and requires 1–3 wt % H_2O. Zeolites precipitate at the highest water contents, varying with protolith composition from as little as 1.6 wt % in the composition of Jake_M to 4–5 wt % in the Bounce Rock and Humphrey compositions. Serpentine precipitation requires at least 2.7 wt % water. This value is relatively constant along the geotherm and therefore gives a good minimum estimate for the amount of water in the Martian subsurface where serpentine is present.

3.4. Modeled Phases Along Geotherms

Figure 4 shows mineral abundances in vol % for the most representative phases modeled, along geotherms of 10 °C/km, 13 °C/km, and 20 °C/km, for the Bounce Rock composition and whole-rock water contents of 2.9 and 4.7 wt %. Actinolite is a ubiquitous phase at all conditions but gradually decreases with increasing metamorphic grade and when prehnite and chlorite are stable phases. At lower water contents, epidote is present along most of the geotherm, thus coexisting with pumpellyite and prehnite (Figures 4a, 4c, and 4e). At higher water contents, epidote precipitates at ~260 °C, producing a phase field where prehnite is stable with chlorite, actinolite, clinopyroxene, albite, and partly with laumontite. This field is larger along the hotter geotherms and is most prominent for 20 °C/km at 4.7 wt % H_2O (Figure 4f). The zeolites stilbite and laumontite are only stable at higher water content with stilbite restricted to the very low *P-T* range along the 10 °C/km and 13 °C/km geotherm (Figures 4b and 4d) and absent along the 20 °C/km geotherm (Figure 4f).

Based on the findings for the composition of Bounce Rock, we extract phase abundances for all other compositions along the 20 °C/km geotherm (Figure 5). The Jake_M composition is dominated by analcime, clinopyroxene, biotite, and albite at both lower (2.9 wt %) and higher (4.5 wt %) water contents. However, the amount of analcime is significantly higher at elevated water levels (Figure 5b). In addition, prehnite is only a stable phase at higher water contents where its coexistence with epidote is limited. For the Humphrey composition, we have extracted phases at higher water contents. At 2.97 wt % H_2O (Figure 5c), the major hydrous phases are actinolite and chlorite, which form the main assemblage together with clinopyroxene and albite. Olivine is still present over the whole *P-T* range. Higher water contents (5.5 wt % H_2O, Figure 5d) result in significantly higher chlorite abundance. Analcime is a stable phase at least up to 350 °C. Neither prehnite nor pumpellyite occur in the Humphrey composition at the studied *P-T* conditions, while epidote stability is restricted to relatively low temperatures and lower amounts of water. The Backstay composition is dominated by albite at lower and higher water content (Figures 5e and 5f). The most abundant hydrous phase is chlorite. Pumpellyite and prehnite are present at higher water content (4.7 wt %, Figure 5f) but not as abundant as in the Bounce Rock composition.

The silica-poor composition is dominated by olivine at a water content of ~3 wt %, while chlorite, amphibole (mainly tremolite), and talc are more abundant hydrous phases than antigorite. At higher water content (5.2 wt % H_2O), antigorite (serpentine) is the dominant hydrous phase while talc is not stable.

4. Discussion

4.1. Limitations of our Model

Our calculations are based on thermodynamic equilibrium, which is not always achieved in realistic geological processes, especially at low temperatures where reaction rates may be slow. However, since we assume a relatively closed system at depth, where fluid is present in pore space with time to react with the subsurface rocks, we consider phase equilibria calculations a good approximation to model low-grade metamorphic processes on Mars. The identification of phases such as prehnite and serpentine on the surface of Mars suggests the availability of a sufficient amount of fluid below the surface to equilibrate low-grade metamorphic assemblages at least locally. We use several simplifications such as calculating with a pure H_2O fluid and not considering CO_2, Cl, and S, as well as variable oxidization states. Deep waters on Earth are expected to increase in salinity (e.g., Möller et al., 1997; Nurmi et al., 1988), resulting in reduced activities of H_2O, which should be addressed in future modeling.

Martian igneous rocks show a large variation of oxygen fugacities ranging from near iron-wüstite to greater than quartz-fayalite-magnetite (Herd, 2006; Schmidt et al., 2013). Additional uncertainties are

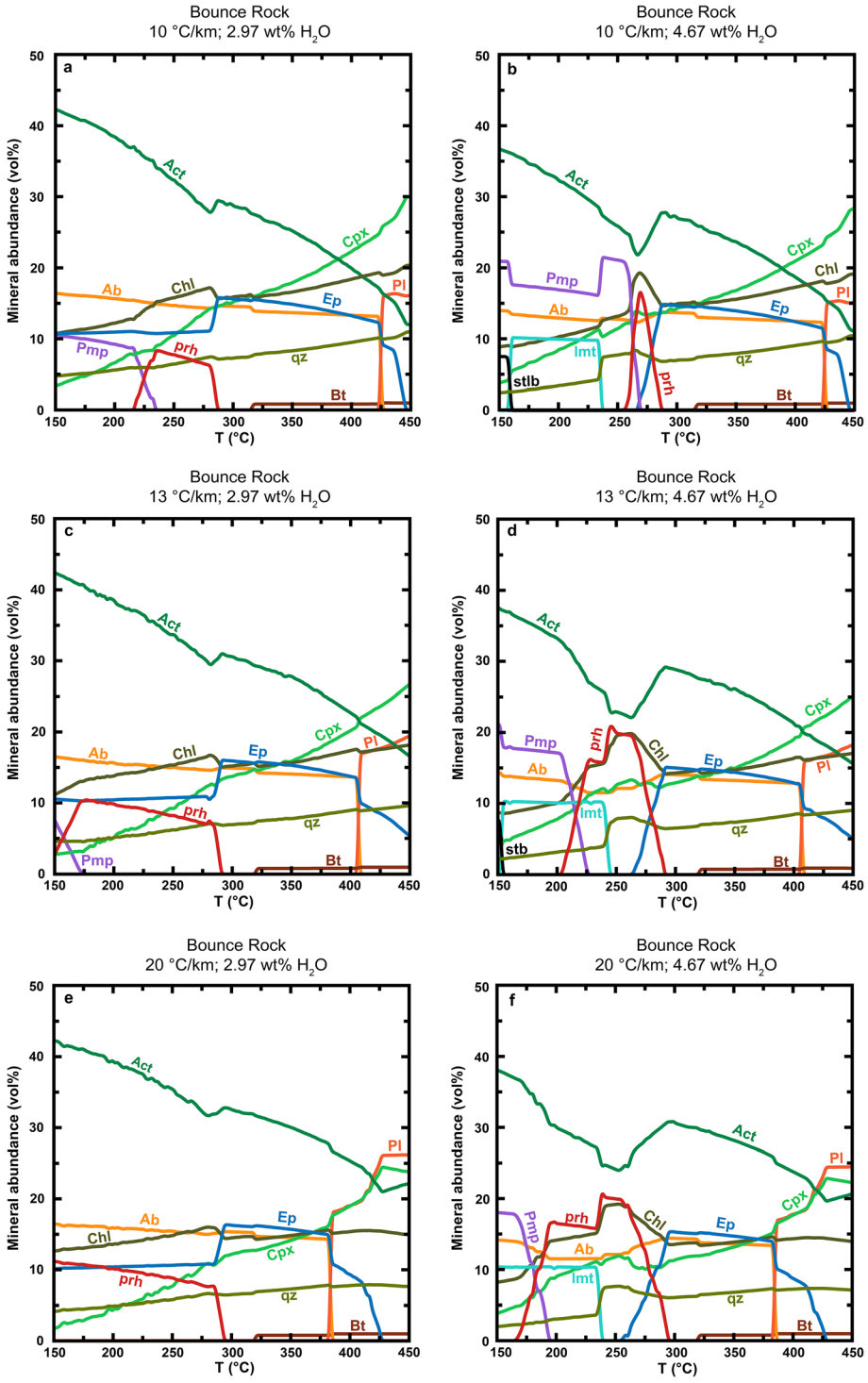

Figure 4. Abundances of common low-grade metamorphic minerals in the Bounce Rock compositions, along geotherms of 10 °C/km, 13 °C/km, and 20 °C/km and fixed water contents of 2.9 and 4.7 wt%. Zeolites are only present for higher water content. Prehnite is stable for all conditions but does coexist with epidote in the assemblage with lower water content. Actinolite is calculated to be abundant for all compositions.

added by the unknown oxygen fugacity during metamorphism, which is influenced by the fluid in addition to the protolith composition, and the error resulting from Fe^{3+}-bearing solid solution models. Addressing this large range of redox conditions is beyond the scope of this work and should be addressed in future modeling.

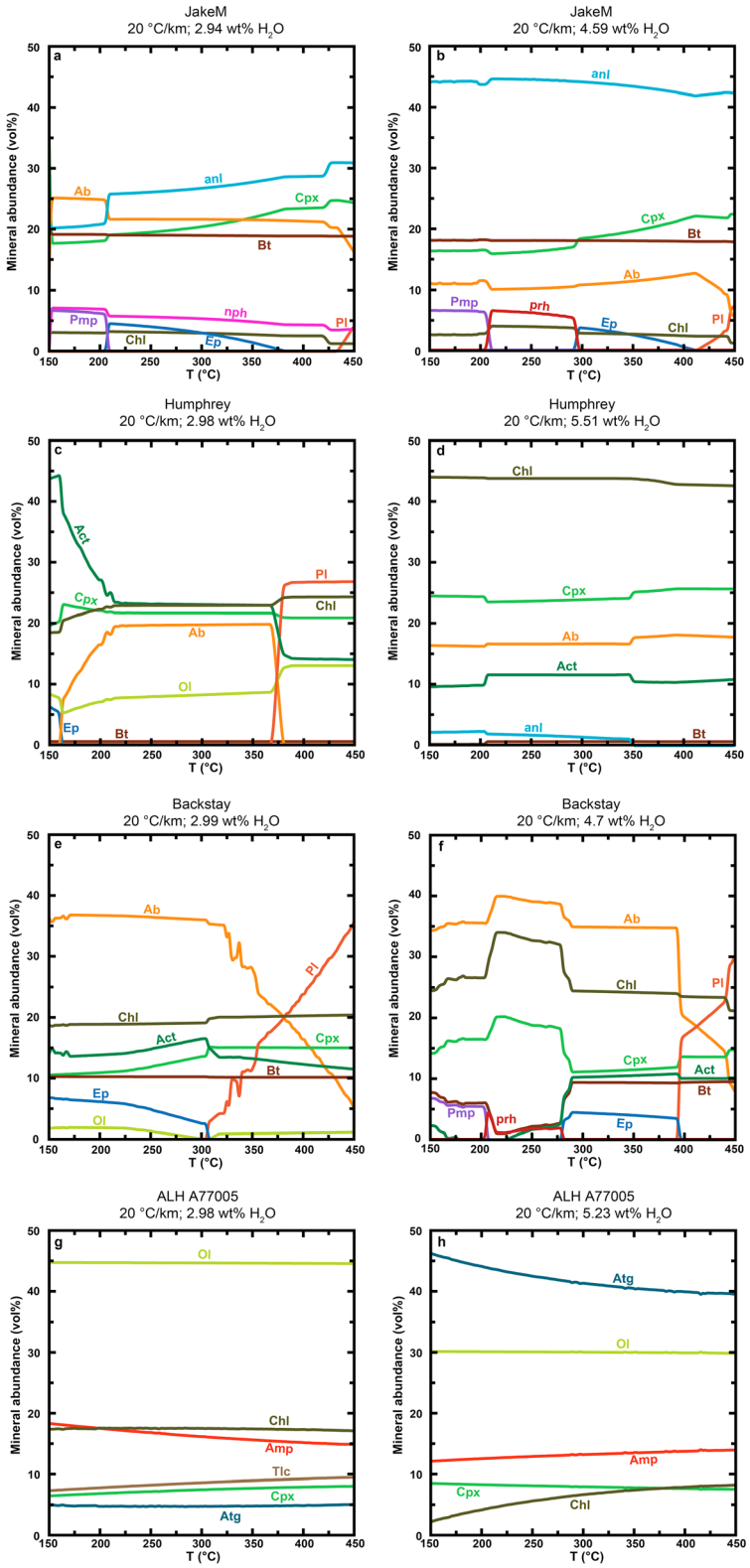

Figure 5. Modal abundance of low-grade metamorphic phases for the compositions of Jake_M, Humphrey, Backstay, and ALH A77005 along a 20 °C/km geotherm at lower and higher water contents. The Jake_M composition yields abundant analcime. Prehnite, pumpellyite, and epidote are not present over most conditions for Humphrey; rather, its metamorphic mineral assemblages are dominated by chlorite, actinolite, and clinopyroxene. The ALHA77005 ultramafic rock composition yields talc at lower water contents, which is replaced by antigorite (serpentine) at higher water contents.

We do not consider some oxides, such as MnO, P_2O_5, and Cr_2O_3, which could influence phase stability fields and mineral abundances, but are not likely to cause fundamental changes in mineralogy. In addition, the models provided rely heavily on, and are therefore limited by, the quality and availability of thermodynamic data and solid solution models, which do not always cover the complete compositional range. Furthermore, the available thermodynamic data has been calibrated for terrestrial compositions and conditions. Mineral stability fields on Mars may therefore deviate from our calculations. Despite these shortcomings, phase equilibria models are still a very useful tool to model phase stabilities for protoliths of variable compositions and provide a more quantitative approach than a comparison of Martian rocks to petrogenetic grids.

4.2. Geothermal Gradient

The majority of detections of hydrated phases are in the southern highlands and Noachian terrains (Ehlmann et al., 2011), although some craters in the northern plains (which are deep enough to sample Noachian basement) have exposed phyllosilicates (e.g., Carter et al., 2013). Based on the occurrence of the vast majority of hydrous phases in Noachian terrains, it has been proposed that most of the hydrous activity was restricted to that time period and that hydrous alteration declined significantly during the Late Noachian, with very little signs for aqueous activity in the younger terrains (Bibring et al., 2006; Carter et al., 2013). For the calculation of progressive metamorphic reactions, we are therefore mostly interested in possible Noachian geotherms.

McSween et al. (2015) calculated a Noachian geotherm of 12 °C/km for the Nili Fossae region. Comparing this geotherm to phase diagrams for terrestrial basaltic rocks, they argue that prehnite would not be a stable phase along this gradient and that at least 16.5 °C/km and >20 °C/km are required to reach the prehnite-pumpellyite and prehnite-actinolite fields, respectively (McSween et al., 2015). Our calculations show, however, that prehnite is a stable phase even along a 10 °C/km geotherm for the Bounce Rock composition (Figures 4a and 4b), although its stability field is limited and it is more abundant along higher geothermal gradients. We find that the restricting factors for colder geotherms are either differences in observed and modeled mineralogy (e.g., presence of epidote together with prehnite at colder geotherms; see section 4.4) or the difficulty in sampling from the greater depths that would be required to precipitate prehnite. For example, the prehnite stability field in the Bounce Rock composition is reached at ~15-km depth along a 13 °C/km geotherm, while only ~8-km depth are required to form prehnite assuming a 20 °C/km (e.g., Figure 1b). Since prehnite has been detected in areas where there is no evidence for tectonic uplift or deep erosion, the mineral has been most likely transported to the surface by cratering (Ehlmann et al., 2011; McSween et al., 2015). Given that the diameters of larger craters range from 50 to 75 km in the Nili Fossae region, the maximum excavation depth would be limited to ~5–8 km (McSween et al., 2015). A hotter geotherm therefore seems more feasible by the possibility of both excavation and mineralogical constraints. However, this does not exclude the possibility of additional heat input provided by hydrothermal activity.

4.3. Hydrothermal System or Prograde Metamorphism With Depth

While VNIR spectroscopy has contributed greatly to the identification of hydrous phases on Mars, there is currently no method to distinguish between minerals formed by hydrothermal alteration versus by low-grade metamorphism, nor is there a means to determine actual mineral assemblages in a rock. In situ measurements by rovers have increased our knowledge of igneous and sedimentary compositions, but to date low-grade metamorphic phases have not been detected. While hydrothermal systems are most likely induced by impact craters (Abramov & Kring, 2005) and are therefore responsible for regional changes in mineralogy (Schwenzer & Kring, 2009, 2013), the implication of progressive metamorphic reactions with depth would be a global change of crustal mineralogy given a sufficient amount of water. The majority of low-grade metamorphic minerals like prehnite, analcime, and serpentine have been found in association with large impact craters (e.g., Carter et al., 2013; Ehlmann et al., 2011). They could either be excavated parts of previously altered crust or have formed by impact-induced hydrothermal systems. The detection of low-grade metamorphic rocks in crater walls and ejecta is seen as an argument for their formation at depth (e.g., Carter et al., 2013). While hydrothermal alteration shows the highest temperatures and intensity around the central uplift, it is highly spatially variable (Schwenzer & Kring, 2013) and may therefore not be distinguishable from prograde metamorphism with depth. On the other hand, the geothermal gradients combined with the estimated excavation depth may not be sufficient to sample low-grade metamorphic minerals from deeper crustal levels. However, multiple cratering events may have brought deeper crustal

rocks to the surface, which may explain the rare occurrence of epidote. The patchy distribution of metamorphic minerals has been associated with hydrothermal activity (McSween et al., 2015). On the other hand, the irregular distribution of hydrous minerals may be a result of various impact events, sampling crustal layers with varying metamorphic grade combined with the incomplete data available about mineral abundance and distribution.

Our calculations show that progressive metamorphism with depth is possible even for colder geotherms, but the presence of phases such as prehnite and serpentine requires at least 2.5 and 2.7 wt % water within the crust. While a hydrothermal system can contribute to higher fluid flow and availability, groundwater and deep crustal fluids could have been present at depths of several kilometers during the Noachian if the ancient geothermal gradient was sufficiently high (Michalski et al., 2013). Due to the lower overburden pressure, pore space on Mars is expected to extend to greater depths than on Earth. Furthermore, permeability, an important factor for subsurface fluid flow, may extend to ~85 km although the permeability-depth variation on Mars is not known (Jones et al., 2011). According to our results, the observed low-grade metamorphic phases could have been formed at relatively low fluid to rock ratios along a geotherm gradient if temperatures were sufficiently high. Additional heat could have been provided by a hydrothermal system or by igneous activity.

4.4. Observed Versus Modeled Phases

In their global survey, Carter et al. (2013) distinguish among nine hydrous spectral classes: (1) Fe/Me phyllosilicates, (2) chlorites, (3) Al-rich smectites/micas, (4) Al-rich kaolins, (5) opaline silica, (6) zeolites/sulfates, (7) serpentines/carbonates, (8) prehnite, and (9) epidote. While prehnite and epidote have very specific absorption features and are easily identified, others such as Fe/Mg phyllosilicates comprise mineral groups with similar cation contents and are therefore difficult to distinguish (Carter et al., 2013). Zeolites and sulfates form in completely different environments but cannot be distinguished very well by their mineral spectra alone. Serpentines and carbonates also share very similar spectral features and have been grouped together although they may form in different environments (Carter et al., 2013). Ehlmann et al. (2009) further distinguish analcime from other zeolites due to its distinctive spectrum. Viviano et al. (2013) identified talc as a possible phase, especially within or close to the olivine-rich terrain in the Nili Fossae area.

To further categorize formation environments, Ehlmann et al. (2011) grouped the observed minerals into assemblages, which seem to be distinctive for certain host craters: (1) prehnite-chlorite-silica, (2) analcime-silica-Fe/Mg-smectite-chlorite, (3) chlorite-illite (muscovite), and (4) serpentine. In this context, an *assemblage* refers to a collection of individual minerals identified in pixels next to each other and not necessarily in the same CRISM pixel (Ehlmann et al., 2011; Viviano et al., 2013). It should also be noted that some minerals do not produce diagnostic spectral signatures in the VNIR wavelength range, such as quartz and feldspars, and can only be detected when hydrated such as opaline silica or contain specific substituents, as in the case of Fe-bearing plagioclase in lunar samples (Ehlmann et al., 2011). Furthermore, a VNIR reflectance spectrum is usually dominated by features from only one or two phases (Ehlmann et al., 2011), while the majority of natural rocks are composed of many minerals, which will be underrepresented when analyzed by remote sensing data alone. The detection of minerals in the spectrum of a pixel or adjacent to each other does not necessarily imply that they originate from the same protolith nor the same formation environment or depth range. This section will focus on the identified and modeled low-grade metamorphic phases rather than clays, sulfates, and carbonates.

4.4.1. Prehnite and Prehnite-Chlorite-Silica

Due to its unique VNIR reflectance spectrum, prehnite can be easily identified and is therefore one of the most characteristic minerals indicative for low-grade metamorphic reactions. Prehnite exposures have been reported globally across Mars, and most of these occurrences are near impact craters (Carter et al., 2013) in ancient terrains (Ehlmann et al., 2011, and references, therein). While the majority of prehnite occurrences also show the presence of chlorite (Ehlmann et al., 2011), prehnite has also been reported to have the strongest spectral signature (Viviano et al., 2013). Our models show that prehnite should form from most protolith compositions (except for Humphrey and the cumulate) at temperatures between ~200 °C to 300 °C (Figures 4 and 5), although slow reaction kinetics may prevent its formation in the lower temperature range. The highest modal abundance of up to 20 vol % is reached in the Bounce Rock composition at

geotherms of 13 °C/km and 20 °C/km (Figures 4d and 4f). These conditions seem to be favorable, as prehnite does not coexist with epidote or pumpellyite, although the latter may be present but difficult to detect by VNIR spectroscopy (see below).

According to our results, prehnite requires at least ~2.5 wt % H_2O to precipitate in Bounce Rock (and possibly higher amounts in other protoliths). This value gives a minimum estimate for the amount of water required in the Martian subsurface, which should be locally available. Prehnite stability is also sensitive to the composition of the fluid phase, with a small amount of CO_2 resulting in the formation of calcite instead of Ca-zeolites and prehnite (McSween et al., 2015). While this makes our assumption of a pure H_2O fluid a valid approximation, the dependence of phase stabilities with fluid variation has to be addressed in future research.

When present in our phase diagrams, prehnite coexists with variable amounts of chlorite in all protolith compositions and both could have been part of a thermally equilibrated assemblage derived from the same protolith. However, chlorite is also an abundant phase in other rock types where prehnite is not a stable phase, for example, the Humphrey composition (Figure 5d), and can be formed by chloritization during diagenetic processes from trioctahedral smectites (e.g., together with illite). It is therefore not a characteristic mineral indicative for specific compositions or conditions, and the detection of chlorite and prehnite in the same spectrum is not a conclusive indicator for both minerals being part of the same assemblage derived from the same protolith. Prehnite and chlorite have also been associated with hydrated silica (Ehlmann et al., 2011), but there is no means to identify specific silica phases. Our calculations show that quartz is a minor component in the Bounce Rock composition over most of the *P-T* range, and its abundance increases with increasing grade due to metamorphic reactions. Quartz is also expected to form by hydrothermal alteration of basaltic protoliths (Schwenzer & Kring, 2013). There is a possibility that quartz has been hydrated after being brought to the surface by impacts or that it is derived from other sources such as altered basaltic glass (Ehlmann et al., 2009). Our model predicts feldspar (albite) and actinolite to be modally more significant parts of the prehnite-chlorite assemblage. While feldspar is difficult to detect by VNIR spectroscopy and is likely present, possible reasons for the nondetection of actinolite are discussed below (section 4.4.3).

4.4.2. Pumpellyite

Pumpellyite has not been detected in VNIR spectra, possibly because its spectrum is very similar to that of Mg-rich chlorite (Ehlmann et al., 2009; Viviano et al., 2013). However, its presence has been inferred from radiative transfer modeling (Poulet et al., 2008) in the central peak of a crater where its modal amount is estimated to be 20%. Our calculations yield similar abundances at higher water contents and colder geotherms (10 °C/km and 13 °C/km) for the Bounce Rock composition (Figures 4b and 4d). For most other compositions and conditions, however, our models do not predict pumpellyite to be a major phase which, combined with its spectral features, may make its detection from orbit difficult. Since pumpellyite is stable at lower temperatures but higher pressures, our models predict it to be more abundant than prehnite along colder geotherms (e.g., Figures 1b, 4b, and 4d). However, it requires more water than prehnite and may therefore not be present in areas of lower water activity. If there is sufficient water to form zeolites by low-grade metamorphic processes, pumpellyite should be a present phase, particularly at temperatures below 250 °C.

4.4.3. Actinolite

Actinolite is a relatively abundant phase in many of our pseudosections (except for the Jake_M and cumulate compositions) and is commonly observed in terrestrial low-grade metamorphic rocks (e.g., Banno, 1998; Bevins & Merriman, 1988; McMullin et al., 2010). Furthermore, it is predicted to be abundant by other thermodynamic models of low-grade metamorphic rocks (Massonne & Willner, 2008; Willner et al., 2013) and should be a part of the assemblage when plotting Martian compositions onto ACF projections (McSween et al., 2015). Although actinolite precipitates at lower water content than prehnite, and should therefore be present in most hydrated Martian compositions, it has not been detected spectrally in areas where prehnite and chlorite have been reported (Carter et al., 2013; Ehlmann et al., 2011). However, it has been identified by CRISM observations together with saponite at Gale crater (Lin et al., 2016). Viviano et al. (2013) demonstrated that talc can be distinguished from the smectite group mineral saponite but has a spectrum similar to that of actinolite. While the presence of actinolite may be less likely than talc in the area studied by Viviano et al. (2013), due to the presence of olivine and absence of pyroxenes, there is the

possibility that it may not have been identified elsewhere because of the similarity of its reflectance spectrum to those of smectites.

Our calculations show that actinolite forms at temperatures below greenschist facies conditions and does not only coexist with epidote but also with many other low-grade metamorphic phases, especially prehnite and pumpellyite. Jake_M is the only composition where it is not stable (Figures 5a and 5b), but this protolith composition is not considered to be widespread on Mars (McSween, 2015) and is therefore not likely to be the origin of all prehnite occurrences detected. Protoliths similar to Backstay (Figure 5f) may contain low amounts of actinolite where prehnite is present (Figure 5f), making it difficult to detect. On the other hand, prehnite is also not an abundant phase at these conditions and is probably less likely to appear in VNIR spectra. Since the range of bulk compositions available is relatively limited, there is also the possibility that the protoliths in the areas where low-grade metamorphic phases have been reported are compositionally different from the protoliths we have studied and actinolite is a less abundant phase. Furthermore, the phase stability of actinolite may be overestimated by the thermodynamic model since it assumes equilibrium even at low temperatures. Terrestrial metabasic volcanic rocks often preserve their textures at low-grade metamorphic conditions resulting in the precipitation of zeolites, prehnite, pumpellyite, chlorite, and epidote in vesicles that are more accessible to fluids (Cho & Liou, 1987; Starkey & Frost, 1990). The first actinolite commonly forms around clinopyroxene phenocrysts within the groundmass (Day & Springer, 2005) and may therefore precipitate later. While this may decrease the modal abundance of the mineral at certain conditions (especially where it is a minor phase), this does not likely destabilize actinolite over the whole *P-T* range and we still expect it to be present for most of the studied compositions as observed in terrestrial analogues. Since it is an abundant mineral even below greenschist-facies conditions, actinolite should not be excluded as a possibility when identifying phases from mineral spectra.

4.4.4. Zeolites

With the exception of analcime, the majority of zeolites cannot easily be spectrally distinguished from sulfates, making the identification of specific minerals difficult (Carter et al., 2013; Ehlmann et al., 2009). Based on the shape and position of certain bands, Carter et al. (2013) conclude that 80% of the minerals detected within the group are zeolites and unspecified zeolites have been reported in the Nili Fossae region (Ehlmann et al., 2009). Zeolites can form in a variety of settings such the interaction of meteoric waters with volcanic rocks, geothermal activity, and at low-grade metamorphic conditions (e.g., Wilkin & Barnes, 1998, and references therein). Since the majority of zeolites is likely formed by surface processes at temperatures below 150 °C, we are not able to model these low-temperature occurrences and will therefore only focus on low-grade metamorphic zeolites. Common zeolites in the modeled metabasic rock compositions are stilbite, laumontite, and wairakite, although the latter requires higher temperatures at low pressure and is not stable along any of the proposed geotherms (Figures 1b, 4, and 5). If the rock composition has enough CaO and H_2O, our calculations predict laumontite to be the most stable zeolite along the chosen geotherms. However, the VNIR reflectance spectrum of laumontite is similar to those of other zeolites (McSween et al., 2015) and may therefore be difficult to be spectrally identified.

4.4.5. Analcime and Analcime-Silica-Smectite-Chlorite

Analcime shows a unique feature in VNIR reflectance spectra and can therefore be distinguished from other zeolites (Ehlmann et al., 2011). It has been detected in a few craters in the Nili Fossae region and is commonly associated with silica, smectites, and chlorite (Ehlmann et al., 2011; Viviano et al., 2013). Analogous with other zeolites, analcime can form by surface, hydrothermal, and low-grade metamorphic processes. The occurrence of hydrated silica in the vicinity has been taken as indicator that analcime formed by near-surface processes or hydrothermal activity rather than low-grade metamorphic reactions (Ehlmann et al., 2011; McSween et al., 2015). In the presence of quartz, analcime dehydrates to albite $+H_2O$ at temperatures below 200 °C and pressures below 0.3 GPa (Liou, 1971). McSween et al. (2015) suggested that the detection of albite (by thermal infrared spectroscopy) near occurrences of analcime (Milam et al., 2010) is an indicator for this dehydration reaction. However, albite is a very common mineral in low-grade metamorphic rocks and would also be an expected phase in the prehnite-chlorite assemblage (e.g., Massonne & Willner, 2008; Willner et al., 2013). The presence of albite therefore cannot be used as a definite indication for analcime dehydration reactions. In the absence of quartz, analcime dehydrates to albite, nepheline, and H_2O at temperatures between 500 °C and 600 °C (Liou, 1971). This is a more likely scenario for our phase equilibria models using basaltic compositions such as Humphrey, where analcime is a stable phase up to

~350 °C (Figure 5d). A very unusual case is the composition of Jake_M (Figures 5a and 5b) where analcime is not only stable over the whole *P-T* range but is also very abundant (>40 vol %) at higher water content (4.5 wt % H_2O; Figure 5b). This is due to the high Na_2O but low CaO content in the whole-rock composition, which destabilizes other Ca-bearing zeolites. Mugearites are relatively rare on Earth, and we do not have a good analogue for its low-grade metamorphic phases. However, analcime-rich mugearites were reported (e.g., Wilkinson & Hensel, 1991) supporting the high modal amounts of analcime in our thermodynamic model.

Ehlmann et al. (2009) noted that locations where they detected hydrated silica and/or analcime correspond to areas that were characterized as *quartzofeldspathic* using thermal infrared spectroscopy (Bandfield, 2006). While Ehlmann et al. (2009) interpret the hydrated silica to be a result of eolian transport, the observed mineralogy could also be derived of a suite of more differentiated magmatic rocks with high amounts of feldspar and phases such as analcime derived from a composition like Jake_M and quartz, which occurs in compositions similar to Bounce Rock.

4.4.6. Epidote

Epidote is a rare phase on Mars and has only been reported in small exposures of a few CRISM pixels (Carter et al., 2013). In terrestrial environments, it forms by hydrothermal processes (e.g., Campos-Alvarez et al., 2010) and under greenschist to amphibolite facies conditions (Willner et al., 2013). It also occurs in contact metamorphic rocks as albite-epidote hornfels and is therefore not always associated with actinolite. Our phase equilibria calculations suggest that epidote forms at temperatures above 250 °C and higher water content for all compositions except for Humphrey and the cumulate (Figures 4 and 5). At lower water availability, however, epidote does seem to be stable toward lower temperatures and even occurs in the Humphrey composition. This is in accordance with results from thermochemical modeling in hydrothermal systems, where epidote is a stable phase in the Humphrey composition at low water/rock ratios (Schwenzer & Kring, 2013). The relative absence of epidote (but presence of prehnite) may therefore be explained by reactions at relatively high water contents and temperatures below ~250 °C for compositions of Bounce Rock, Jake_M, and Backstay, and temperatures above ~170 °C at any water content for Humphrey. Alternatively, epidote may not always be a detectable phase, as its abundance is limited to <5 vol % in compositions similar to Backstay and Jake_M.

4.4.7. Serpentine

Serpentine is often found in close proximity with pure or mixed olivine spectra (Carter et al., 2013) and was detected both in crater materials and in bedrock units (Viviano et al., 2013). Serpentine formation is a result of hydration of ultramafic rocks and requires ~2.7 wt % of water according to our models. However, at ~3 wt% H_2O, it is not the most abundant hydrous phase and chlorite, amphibole, and talc are more common (Figure 5g). The relatively low abundance of serpentine at lower water content may make its detection difficult despite it being present in the rock and may not necessarily imply a dry rock composition. When present, serpentine is often associated with magnesium carbonates (Ehlmann et al., 2009), although a discrimination between the two is made difficult by similar features of their spectra (Carter et al., 2013). In the presence of a CO_2-bearing fluid magnesite should be formed in ultramafic rocks rather than brucite, which has to be addressed in future research.

4.4.8. Talc

Based on findings from talc deposit spectra in the Pilbara region, Australia, Brown et al. (2010) suggested that talc may be present instead of saponite in the olivine-rich region of the Nili Fossae area. By further scrutinizing mineral spectra, Viviano et al. (2013) concluded that talc is distinguishable from saponite and may be a possible and probable phase particularly where associated with carbonates. It is noteworthy, however, that the VNIR reflectance spectrum of actinolite resembles that of talc (see section 4.4.3). The formation of talc and magnesite has been associated with carbonation of serpentine in the presence of CO_2 (Viviano et al., 2013). Complete carbonation of serpentinite seems to be most effective at small fluid to rock ratios and temperatures below 200 °C, while higher fluid flux at these temperatures can result in decarbonation and silicification processes and carbonation is less likely at higher temperatures even at higher fluid to rock ratios (Klein & Garrido, 2011). While this seems a probable process on Mars given the availability of CO_2 in the atmosphere and the low temperatures, our phase equilibria models provide an alternative, where the presence of talc is restricted by the water content of the rock (0.9–4.7 wt % H_2O). However, the influence of a variable fluid composition on talc stability has not been investigated and has to be addressed in future models.

5. Conclusions

Using phase equilibria models, we can show that compositional differences in Martian protoliths greatly influence phase stability fields for low-grade metamorphic rocks. Our models reproduce all low-grade metamorphic hydrous minerals like prehnite, chlorite, unspecified zeolites, analcime, and serpentine, which have been detected on Mars by visible/near-infrared spectroscopy. Prehnite, the most characteristic low-grade metamorphic mineral reported up to date does form in most (but not all mafic) compositions and where present requires at least 2.5 wt % water in the system. Serpentine is restricted to ultramafic compositions and forms at >2.7 wt % water. In compositions with higher CaO, zeolites such as stilbite and laumontite are present, whereas lower CaO results in the presence of analcime. Alteration minerals from the composition of the Martian mugearite, Jake_M, include very high proportions of analcime. Pumpellyite may be present, especially at lower temperatures, but its VNIR spectrum is difficult to distinguish from that of chlorite. By thermodynamic constraints, actinolite should be a stable phase at most low-grade metamorphic conditions, but it may be difficult to detect in VNIR spectra. Talc could be present as a result of restricted water content in addition to a carbonation reaction of serpentine. While prehnite does form along colder geothermal gradients of 10 °C/km and 13 °C/km, the presence of a hotter geotherm of 20 °C/km is more likely due to the restricted excavation depth of larger craters ranging between 5 and 8 km. Alternatively, additional heat could have been provided by a hydrothermal system or volcanic activity. The effect of variations in fluid composition and oxygen fugacity on phase stabilities has yet to be addressed by thermodynamic modeling.

Acknowledgments
This work was supported through the Graham Ryder Fellowship granted to J. S. by USRA at the LPI. Additional phase diagrams and mineral abundance tables for Figures and are available as supporting information. We are grateful for reviews by H. Y. McSween and M. Schmidt and editorial handling by D. Baratoux. This is LPI contribution number LPI-2155.

References

Abramov, O., & Kring, D. A. (2005). Impact-induced hydrothermal activity on early Mars. *Journal of Geophysical Research*, *110*, E12S09. https://doi.org/10.1029/2005JE002453

Agee, C. B., Wilson, N. V., McCubbin, F. M., Ziegler, K., Polyak, V. J., Sharp, Z. D., et al. (2013). Unique meteorite from Early Amazonian Mars: Water-rich basaltic breccia Northwest Africa 7034. *Science*, *339*(6121), 780–785. https://doi.org/10.1126/science.1228858

Arvidson, R. E., Squyres, S. W., Bell, J. F., Catalano, J. G., Clark, B. C., Crumpler, L. S., et al. (2014). Ancient aqueous environments at Endeavour Crater, Mars. *Science*, *343*(6169), 1248097. https://doi.org/10.1126/science.1248097

Bandfield, J. L. (2006). Extended surface exposures of granitoid compositions in Syrtis Major, Mars. *Geophysical Research Letters*, *33*, L06203. https://doi.org/10.1029/2005GL025559

Banno, S. (1998). Pumpellyite–actinolite facies of the Sanbagawa metamorphism. *Journal of Metamorphic Geology*, *16*(1), 117–128. https://doi.org/10.1111/j.1525-1314.1998.00071.x

Bevins, R. E., & Merriman, R. J. (1988). Compositional controls on coexisting prehnite-actinolite and prehnite-pumpellyite facies assemblages in the Tal y Fan metabasite intrusion, North Wales: Implications for Caledonian metamorphic field gradients. *Journal of Metamorphic Geology*, *6*(1), 17–39. https://doi.org/10.1111/j.1525-1314.1988.tb00406.x

Bibring, J.-P., Langevin, Y., Mustard, J. F., Poulet, F., Arvidson, R., Gendrin, A., Gondet, B., et al. (2006). Global mineralogical and aqueous Mars history derived from OMEGA/Mars Express data. *Science*, *312*(5772), 400–404. https://doi.org/10.1126/science.1122659

Boynton, W. V., Taylor, G. J., Evans, L. G., Reedy, R. C., Starr, R., Janes, D. M., et al. (2007). Concentration of H, Si, Cl, K, Fe, and Th in the low- and mid-latitude regions of Mars. *Journal of Geophysical Research*, *112*, E12S99. https://doi.org/10.1029/2007JE002887

Bridges, J. C., & Schwenzer, S. P. (2012). The nakhlite hydrothermal brine on Mars. *Earth and Planetary Science Letters*, *359-360*, 117–123. https://doi.org/10.1016/j.epsl.2012.09.044

Bridges, J. C., Schwenzer, S. P., Leveille, R., Westall, F., Wiens, R. C., Mangold, N., et al. (2015). Diagenesis and clay mineral formation at Gale crater, Mars. *Journal of Geophysical Research: Planets*, *120*, 1–19. https://doi.org/10.1002/2014JE004757

Bridges, J. C., & Warren, P. H. (2006). The SNC meteorites: Basaltic igneous processes on Mars. *Journal of the Geological Society*, *163*(2), 229–251. https://doi.org/10.1144/0016-764904-501

Brown, A. J., Hook, S. J., Baldridge, A. M., Crowley, J. K., Bridges, N. T., Thomson, B. J., et al. (2010). Hydrothermal formation of clay-carbonate alteration assemblages in the Nili Fossae region of Mars. *Earth and Planetary Science Letters*, *297*(1-2), 174–182. https://doi.org/10.1016/j.epsl.2010.06.018

Brückner, J., Dreibus, G., Rieder, R., & Wänke, H. (2003). Refined data of Alpha Proton X-ray Spectrometer analyses of soils and rocks at the Mars Pathfinder site: Implications for surface chemistry. *Journal of Geophysical Research*, *108*(E12), 8094. https://doi.org/10.1029/2003JE002060

Campos-Alvarez, N. O., Samson, I. M., Fryer, B. J., & Ames, D. E. (2010). Fluid sources and hydrothermal architecture of the Sudbury Structure: Constraints from femtosecond LA-MC-ICP-MS Sr isotopic analysis of hydrothermal epidote and calcite. *Chemical Geology*, *278*(3-4), 131–150. https://doi.org/10.1016/j.chemgeo.2010.09.006

Carr, M. H., & Head, J. W. III (2010). Geologic history of Mars. *Earth and Planetary Science Letters*, *294*(3–4), 185–203. https://doi.org/10.1016/j.epsl.2009.06.042

Carrozzo, F. G., Di Achille, G., Salese, F., Altieri, F., & Bellucci, G. (2017). Geology and mineralogy of the Auki Crater, Tyrrhena Terra, Mars: A possible post impact-induced hydrothermal system. *Icarus*, *281*, 228–239. https://doi.org/10.1016/j.icarus.2016.09.001

Carter, J., Poulet, F., Bibring, J.-P., Mangold, N., & Murchie, S. L. (2013). Hydrous minerals on Mars as seen by the CRISM and OMEGA imaging spectrometers: Updated global view. *Journal of Geophysical Research: Planets*, *118*, 831–858. https://doi.org/10.1029/2012JE004145

Changela, H. G., & Bridges, J. C. (2010). Alteration assemblages in the nakhlites: Variation with depth on Mars. *Meteoritics & Planetary Science*, *45*(12), 1847–1867. https://doi.org/10.1111/j.1945-5100.2010.01123.x

Cho, M., & Liou, J. G. (1987). Prehnite-pumpellyite to greenschist fades transition in the Karmutsen Metabasites, Vancouver Island, B.C. *Journal of Petrology*, *28*(3), 417–443. https://doi.org/10.1093/petrology/28.3.417

Christensen, P. R., Bandfield, J. L., Hamilton, V. E., Ruff, S. W., Kieffer, H. H., Titus, T. N., et al. (2001). Mars Global Surveyor Thermal Emission Spectrometer experiment: Investigation description and surface science results. *Journal of Geophysical Research*, *106*(E10), 23,823–23,871. https://doi.org/10.1029/2000JE001370

Connolly, J. A. D. (2005). Computation of phase equilibria by linear programming: A tool for geodynamic modeling and its application to subduction zone decarbonation. *Earth and Planetary Science Letters*, *236*, 524–541. https://doi.org/10.1016/j.epsl.2005.04.033

Day, H. W., & Springer, R. K. (2005). The first appearance of actinolite in the prehnite–pumpellyite facies, Sierra Nevada, California. *The Canadian Mineralogist*, *43*(1), 89–104. https://doi.org/10.2113/gscanmin.43.1.89

Ehlmann, B. L., Mustard, J. F., Clark, R. N., Swayze, G. A., & Murchie, S. L. (2011). Evidence for low-grade metamorphism, hydrothermal alteration, and diagenesis on Mars from phyllosilicate mineral assemblages. *Clays and Clay Minerals*, *59*(4), 359–377. https://doi.org/10.1346/CCMN.2011.0590402

Ehlmann, B. L., Mustard, J. F., Swayze, G. A., Clark, R. N., Bishop, J. L., Poulet, F., et al. (2009). Identification of hydrated silicate minerals on Mars using MRO-CRISM: Geologic context near Nili Fossae and implications for aqueous alteration. *Journal of Geophysical Research*, *114*, E00D08. https://doi.org/10.1029/2009JE003339

Fassett, C. I., & Head, J. W. (2008). Valley network-fed, open-basin lakes on Mars: Distribution and implications for Noachian surface and subsurface hydrology. *Icarus*, *198*(1), 37–56. https://doi.org/10.1016/j.icarus.2008.06.016

Filiberto, J., & Schwenzer, S. P. (2013). Alteration mineralogy of Home Plate and Columbia Hills—Formation conditions in context to impact, volcanism, and fluvial activity. *Meteoritics & Planetary Science*, *48*(10), 1937–1957. https://doi.org/10.1111/maps.12207

Filiberto, J., Treiman, A. H., Giesting, P. A., Goodrich, C. A., & Gross, J. (2014). High-temperature chlorine-rich fluid in the martian crust: A precursor to habitability. *Earth and Planetary Science Letters*, *401*, 110–115. https://doi.org/10.1016/j.epsl.2014.06.003

Filiberto, J., Treiman, A. H., & Le, L. (2008). Crystallization experiments on a Gusev Adirondack basalt composition. *Meteoritics & Planetary Science*, *43*(7), 1137–1146. https://doi.org/10.1111/j.1945-5100.2008.tb01118.x

Flahaut, J., Quantin, C., Clenet, H., Allemand, P., Mustard, J. F., & Thomas, P. (2012). Pristine Noachian crust and key geologic transitions in the lower walls of Valles Marineris: Insights into early igneous processes on Mars. *Icarus*, *221*(1), 420–435. https://doi.org/10.1016/j.icarus.2011.12.027

Frey, M., Capitani, C. D., & Liou, J. G. (1991). A new petrogenetic grid for low-grade metabasites. *Journal of Metamorphic Geology*, *9*(4), 497–509. https://doi.org/10.1111/j.1525-1314.1991.tb00542.x

Gale, A., Dalton, C. A., Langmuir, C. H., Su, Y., & Schilling, J.-G. (2013). The mean composition of ocean ridge basalts. *Geochemistry, Geophysics, Geosystems*, *14*, 489–518. https://doi.org/10.1029/2012GC004334

Gellert, R., Rieder, R., Brückner, J., Clark, B. C., Dreibus, G., Klingelhöfer, G., et al. (2006). Alpha Particle X-Ray Spectrometer (APXS): Results from Gusev crater and calibration report. *Journal of Geophysical Research*, *111*, E02S05. https://doi.org/10.1029/2005JE002555

Gendrin, A., Mangold, N., Bibring, J.-P., Langevin, Y., Gondet, B., Poulet, F., et al. (2005). Sulfates in Martian layered terrains: The OMEGA/Mars Express view. *Science*, *307*(5715), 1587–1591. https://doi.org/10.1126/science.1109087

Giesting, P. A., & Filiberto, J. (2016). The formation environment of potassic-chloro-hastingsite in the nakhlites MIL 03346 and pairs and NWA 5790: Insights from terrestrial chloro-amphibole. *Meteoritics & Planetary Science*, *51*(11), 2127–2153. https://doi.org/10.1111/maps.12675

Griffith, L. L., & Shock, E. L. (1997). Hydrothermal hydration of Martian crust: Illustration via geochemical model calculations. *Journal of Geophysical Research*, *102*(E4), 9135–9143. https://doi.org/10.1029/96JE02939

Harrison, K. P., & Grimm, R. E. (2005). Groundwater-controlled valley networks and the decline of surface runoff on early Mars. *Journal of Geophysical Research*, *110*, E12S16. https://doi.org/10.1029/2005JE002455

Herd, C. D. K. (2006). Insights into the redox history of the NWA 1068/1110 Martian basalt from mineral equilibria and vanadium oxybarometry. *American Mineralogist*, *91*(10), 1616–1627. https://doi.org/10.2138/am.2006.2104

Hicks, L. J., Bridges, J. C., & Gurman, S. J. (2014). Ferric saponite and serpentine in the nakhlite Martian meteorites. *Geochimica et Cosmochimica Acta*, *136*, 194–210. https://doi.org/10.1016/j.gca.2014.04.010

Holland, T. J. B., & Powell, R. (1996). Thermodynamics of order-disorder in minerals: II. Symmetric formalism applied to solid solutions. *American Mineralogist*, *81*(11-12), 1425–1437. https://doi.org/10.2138/am-1996-11-1215

Holland, T. J. B., & Powell, R. (1998). An internally consistent thermodynamic data set for phases of petrological interest. *Journal of Metamorphic Geology*, *16*, 309–343.

Holland, T. J. B., & Powell, R. (2011). An improved and extended internally consistent thermodynamic dataset for phases of petrological interest, involving a new equation of state for solids. *Journal of Metamorphic Geology*, *29*, 333–383. https://doi.org/j.1525-1314.2010.00923.x

Howard, A. D., Moore, J. M., & Irwin, R. P. (2005). An intense terminal epoch of widespread fluvial activity on early Mars: 1. Valley network incision and associated deposits. *Journal of Geophysical Research*, *110*, E12S14. https://doi.org/10.1029/2005JE002459

Irwin, R. P., Howard, A. D., Craddock, R. A., & Moore, J. M. (2005). An intense terminal epoch of widespread fluvial activity on early Mars: 2. Increased runoff and paleolake development. *Journal of Geophysical Research*, *110*, E12S15. https://doi.org/10.1029/2005JE002460

Jones, E. G., Lineweaver, C. H., & Clarke, J. D. (2011). An extensive phase space for the potential Martian biosphere. *Astrobiology*, *11*(10), 1017–1033. https://doi.org/10.1089/ast.2011.0660

Klein, F., & Garrido, C. J. (2011). Thermodynamic constraints on mineral carbonation of serpentinized peridotite. *Lithos*, *126*(3-4), 147–160. https://doi.org/10.1016/j.lithos.2011.07.020

Lin, H., Zhang, X., Shuai, T., Zhang, L., & Sun, Y. (2016). Abundance retrieval of hydrous minerals around the Mars Science Laboratory landing site in Gale crater, Mars. *Planetary and Space Science*, *121*, 76–82. https://doi.org/10.1016/j.pss.2015.12.007

Liou, J. G. (1971). Analcime equilibria. *Lithos*, *4*(4), 389–402. https://doi.org/10.1016/0024-4937(71)90122-8

Lodders, K. (1998). A survey of shergottite, nakhlite and chassigny meteorites whole-rock compositions. *Meteoritics & Planetary Science*, *33*(S4), A183–A190. https://doi.org/10.1111/j.1945-5100.1998.tb01331.x

Loizeau, D., Carter, J., Bouley, S., Mangold, N., Poulet, F., Bibring, J.-P., et al. (2012). Characterization of hydrated silicate-bearing outcrops in Tyrrhena Terra, Mars: Implications to the alteration history of Mars. *Icarus*, *219*(1), 476–497. https://doi.org/10.1016/j.icarus.2012.03.017

Mangold, N., Carter, J., Poulet, F., Dehouck, E., Ansan, V., & Loizeau, D. (2012). Late Hesperian aqueous alteration at Majuro crater, Mars. *Planetary and Space Science*, *72*(1), 18–30. https://doi.org/10.1016/j.pss.2012.03.014

Marzo, G. A., Davila, A. F., Tornabene, L. L., Dohm, J. M., Fairén, A. G., Gross, C., et al. (2010). Evidence for Hesperian impact-induced hydrothermalism on Mars. *Icarus*, *208*(2), 667–683. https://doi.org/10.1016/j.icarus.2010.03.013

Massonne, H.-J. (2010). Phase relations and dehydration behaviour of calcareous sediments at very-low to low grade metamorphic conditions. *Periodico Di Mineralogia*, *79*, 21–43.

Massonne, H.-J., & Willner, A. P. (2008). Phase relations and dehydration behaviour of psammopelite and mid-ocean ridge basalt at very-low-grade to low-grade metamorphic conditions. *European Journal of Mineralogy*, *20*(5), 867–879. https://doi.org/10.1127/0935-1221/2008/0020-1871

McGovern, P. J., Solomon, S. C., Smith, D. E., Zuber, M. T., Simons, M., Wieczorek, M. A., et al. (2004). Correction to "Localized gravity/topography admittance and correlation spectra on Mars: Implications for regional and global evolution" - McGovern - 2004 - journal of geophysical research: Planets - Wiley online library. *Journal of Geophysical Research*, *109*, E07007. Retrieved from https://agupubs.onlinelibrary.wiley.com/, https://doi.org/10.1029/2004JE002286

McMullin, D. W. A., Barr, S. M., & Raeside, R. P. (2010). Very low- and low-grade metamorphism of mafic volcanic rocks of the Mira terrane (Avalonia), southeastern Cape Breton Island, Nova Scotia. *Atlantic Geology*, *46*(0), 95–126. https://doi.org/10.4138/atlgeol.2010.006

McSween, H. Y. (2015). Petrology on Mars. *American Mineralogist*, *100*(11–12), 2380–2395. https://doi.org/10.2138/am-2015-5257

McSween, H. Y., Arvidson, R. E., Bell, J. F., Blaney, D., Cabrol, N. A., Christensen, P. R., et al. (2004). Basaltic rocks analyzed by the Spirit rover in Gusev crater. *Science*, *305*(5685), 842–845. https://doi.org/10.1126/science.3050842

McSween, H. Y., Labotka, T. C., & Viviano-Beck, C. E. (2015). Metamorphism in the Martian crust. *Meteoritics & Planetary Science*, *50*(4), 590–603. https://doi.org/10.1111/maps.12330

McSween, H. Y., Ruff, S. W., Morris, R. V., Bell, J. F., Herkenhoff, K., Gellert, R., et al. (2006). Alkaline volcanic rocks from the Columbia Hills, Gusev crater, Mars. *Journal of Geophysical Research*, *111*, E09S91. https://doi.org/10.1029/2006JE002698

Meyer, C. (2013). The Martian meteorite compendium. Retrieved from https://curator.jsc.nasa.gov/antmet/mmc/contents.cfm

Michalski, J. R., Cuadros, J., Niles, P. B., Parnell, J., Rogers, A. D., & Wright, S. P. (2013). Groundwater activity on Mars and implications for a deep biosphere. *Nature Geoscience*, *6*(2), 133–138. https://doi.org/10.1038/ngeo1706

Milam, K. A., McSween, H. Y., Moersch, J., & Christensen, P. R. (2010). Distribution and variation of plagioclase compositions on Mars. *Journal of Geophysical Research*, *115*, E09004. https://doi.org/10.1029/2009JE003495

Milliken, R. E., Swayze, G. A., Arvidson, R. E., Bishop, J. L., Clark, R. N., Ehlmann, B. L., et al. (2008). Opaline silica in young deposits on Mars. *Geology*, *36*(11), 847–850. https://doi.org/10.1130/G24967A.1

Ming, D. W., Gellert, R., Morris, R. V., Arvidson, R. E., Brückner, J., Clark, B. C., et al. (2008). Geochemical properties of rocks and soils in Gusev crater, Mars: Results of the Alpha Particle X-Ray Spectrometer from Cumberland Ridge to Home Plate. *Journal of Geophysical Research*, *113*, E12S39. https://doi.org/10.1029/2008JE003195

Mitrofanov, I. G., Litvak, M. L., Sanin, A. B., Starr, R. D., Lisov, D. I., Kuzmin, R. O., et al. (2014). Water and chlorine content in the Martian soil along the first 1900 m of the Curiosity rover traverse as estimated by the DAN instrument. *Journal of Geophysical Research: Planets*, *119*, 1579–1596. https://doi.org/10.1002/2013JE004553

Möller, P., Weise, S. M., Althaus, E., Bach, W., Behr, H. J., Borchardt, R., et al. (1997). Paleofluids and recent fluids in the upper continental crust: Results from the German Continental Deep Drilling Program (KTB). *Journal of Geophysical Research*, *102*(B8), 18,233–18,254. https://doi.org/10.1029/96JB02899

Murchie, S. L., Arvidson, R., Bedini, P., Beisser, K., Bibring, J.-P., Bishop, J., et al. (2007). Compact Reconnaissance Imaging Spectrometer for Mars (CRISM) on Mars Reconnaissance Orbiter (MRO). *Journal of Geophysical Research*, *112*, E05S03. https://doi.org/10.1029/2006JE002682

Murchie, S. L., Mustard, J. F., Ehlmann, B. L., Milliken, R. E., Bishop, J. L., McKeown, N. K., et al. (2009). A synthesis of Martian aqueous mineralogy after 1 Mars year of observations from the Mars Reconnaissance Orbiter. *Journal of Geophysical Research*, *114*, E00D06. https://doi.org/10.1029/2009JE003342

Mustard, J. F., Murchie, S. L., Pelkey, S. M., Ehlmann, B. L., Milliken, R. E., Grant, J. A., et al. (2008). Hydrated silicate minerals on Mars observed by the Mars Reconnaissance Orbiter CRISM instrument. *Nature*, *454*(7202), 305–309. https://doi.org/10.1038/nature07097

Newton, R. C., Charlu, T. V., & Kleppa, O. J. (1980). Thermochemistry of the high structural state plagioclases. *Geochimica et Cosmochimica Acta*, *44*(7), 933–941. https://doi.org/10.1016/0016-7037(80)90283-5

Nurmi, P. A., Kukkonen, I. T., & Lahermo, P. W. (1988). Geochemistry and origin of saline groundwaters in the Fennoscandian Shield. *Applied Geochemistry*, *3*(2), 185–203. https://doi.org/10.1016/0883-2927(88)90007-8

Osinski, G. R., Tornabene, L. L., Banerjee, N. R., Cockell, C. S., Flemming, R., Izawa, M. R. M., et al. (2013). Impact-generated hydrothermal systems on Earth and Mars. *Icarus*, *224*(2), 347–363. https://doi.org/10.1016/j.icarus.2012.08.030

Padrón-Navarta, J. A., Sánchez-Vizcaíno, V. L., Hermann, J., Connolly, J. A. D., Garrido, C. J., Gómez-Pugnaire, M. T., & Marchesi, C. (2013). Tschermak's substitution in antigorite and consequences for phase relations and water liberation in high-grade serpentinites. *Lithos*, *178*, 186–196. https://doi.org/10.1016/j.lithos.2013.02.001

Parmentier, E. M., & Zuber, M. T. (2007). Early evolution of Mars with mantle compositional stratification or hydrothermal crustal cooling. *Journal of Geophysical Research*, *112*, E02007. https://doi.org/10.1029/2005JE002626

Poulet, F., Bibring, J.-P., Mustard, J. F., Gendrin, A., Mangold, N., Langevin, Y., et al., & The Omega Team (2005). Phyllosilicates on Mars and implications for early Martian climate. *Nature*, *438*(7068), 623–627. https://doi.org/10.1038/nature04274

Poulet, F., Mangold, N., Loizeau, D., Bibring, J.-P., Langevin, Y., Michalski, J., & Gondet, B. (2008). Abundance of minerals in the phyllosilicate-rich units on Mars. *Astronomy & Astrophysics*, *487*(2), L41–L44. https://doi.org/10.1051/0004-6361:200810150

Schmidt, M. E., Campbell, J. L., Gellert, R., Perrett, G. M., Treiman, A. H., Blaney, D. L., et al. (2014). Geochemical diversity in first rocks examined by the Curiosity Rover in Gale crater: Evidence for and significance of an alkali and volatile-rich igneous source. *Journal of Geophysical Research: Planets*, *119*, 64–81. https://doi.org/10.1002/2013JE004481

Schmidt, M. E., Perrett, G. M., Bray, S. L., Bradley, N. J., Lee, R. E., Berger, J. A., et al. (2018). Dusty rocks in Gale crater: Assessing areal coverage and separating dust and rock contributions in APXS analyses. *Journal of Geophysical Research: Planets*, *123*, 1649–1673. https://doi.org/10.1029/2018JE005553

Schmidt, M. E., Schrader, C. M., & McCoy, T. J. (2013). The primary fO2 of basalts examined by the Spirit rover in Gusev crater, Mars: Evidence for multiple redox states in the Martian interior. *Earth and Planetary Science Letters*, *384*, 198–208. https://doi.org/10.1016/j.epsl.2013.10.005

Schwenzer, S. P., Bridges, J. C., Wiens, R. C., Conrad, P. G., Kelley, S. P., Leveille, R., et al. (2016). Fluids during diagenesis and sulfate vein formation in sediments at Gale crater, Mars. *Meteoritics & Planetary Science*, *51*(11), 2175–2202. https://doi.org/10.1111/maps.12668

Schwenzer, S. P., & Kring, D. A. (2009). Impact-generated hydrothermal systems capable of forming phyllosilicates on Noachian Mars. *Geology*, *37*(12), 1091–1094. https://doi.org/10.1130/G30340A.1

Schwenzer, S. P., & Kring, D. A. (2013). Alteration minerals in impact-generated hydrothermal systems—Exploring host rock variability. *Icarus*, *226*(1), 487–496. https://doi.org/10.1016/j.icarus.2013.06.003

Squyres, S. W., Arvidson, R. E., Bell, J. F., Calef, F., Clark, B. C., Cohen, B. A., et al. (2012). Ancient impact and aqueous processes at Endeavour crater, Mars. *Science*, *336*(6081), 570–576. https://doi.org/10.1126/science.1220476

Squyres, S. W., Arvidson, R. E., Ruff, S., Gellert, R., Morris, R. V., Ming, D. W., et al. (2008). Detection of silica-rich deposits on Mars. *Science*, *320*(5879), 1063–1067. https://doi.org/10.1126/science.1155429

Starkey, R. J., & Frost, B. R. (1990). Low-grade metamorphism of the Karmutsen Volcanics, Vancouver Island, British Columbia. *Journal of Petrology*, *31*(1), 167–195. https://doi.org/10.1093/petrology/31.1.167

Stolper, E. M., Baker, M. B., Newcombe, M. E., Schmidt, M. E., Treiman, A. H., Cousin, A., et al. (2013). The petrochemistry of Jake_M: A Martian mugearite. *Science*, *341*(6153), 1239463. https://doi.org/10.1126/science.1239463

Sun, V. Z., & Milliken, R. E. (2015). Ancient and recent clay formation on Mars as revealed from a global survey of hydrous minerals in crater central peaks. *Journal of Geophysical Research: Planets*, *120*, 2293–2332. https://doi.org/10.1002/2015JE004918

Tajčmanová, L., Connolly, J. A. D., & Cesare, B. (2009). A thermodynamic model for titanium and ferric iron solution in biotite. *Journal of Metamorphic Geology*, *27*(2), 153–165. https://doi.org/10.1111/j.1525-1314.2009.00812.x

Thompson, J. B., & Waldbaum, D. R. (1969). Mixing properties of sanidine crystalline solutions: III. Calculations based on two-phase data. *American Mineralogist*, *54*(5–6), 811–838.

Treiman, A. H. (2005). The nakhlite meteorites: Augite-rich igneous rocks from Mars. *Chemie der Erde - Geochemistry*, *65*(3), 203–270. https://doi.org/10.1016/j.chemer.2005.01.004

Treiman, A. H., & Filiberto, J. (2015). Geochemical diversity of shergottite basalts: Mixing and fractionation, and their relation to Mars surface basalts. *Meteoritics & Planetary Science*, *50*(4), 632–648. https://doi.org/10.1111/maps.12363

Turcotte, D. L., Shcherbakov, R., Malamud, B. D., & Kucinskas, A. B. (2002). Is the Martian crust also the Martian elastic lithosphere? *Journal of Geophysical Research*, *107*(E11), 5091. Retrieved from https://agupubs.onlinelibrary.wiley.com/doi/abs/, https://doi.org/10.1029/2001JE001594

Vaniman, D. T., Bish, D. L., Ming, D. W., Bristow, T. F., Morris, R. V., Blake, D. F., et al. (2014). Mineralogy of a mudstone at Yellowknife Bay, Gale crater, Mars. *Science*, *343*(6169), 1243480. https://doi.org/10.1126/science.1243480

Viviano, C. E., Moersch, J. E., & McSween, H. Y. (2013). Implications for early hydrothermal environments on Mars through the spectral evidence for carbonation and chloritization reactions in the Nili fossae region. *Journal of Geophysical Research: Planets*, *118*, 1858–1872. https://doi.org/10.1002/jgre.20141

Wei, C., & Powell, R. (2003). Phase relations in high-pressure metapelites in the system KFMASH (K_2O–FeO–MgO–Al_2O_3–SiO_2–H_2O) with application to natural rocks. *Contributions to Mineralogy and Petrology*, *145*(3), 301–315. https://doi.org/10.1007/s00410-003-0454-1

White, R. W., Powell, R., Holland, T. J. B., Johnson, T. E., & Green, E. C. R. (2014). New mineral activity–composition relations for thermodynamic calculations in metapelitic systems. *Journal of Metamorphic Geology*, *32*(3), 261–286. https://doi.org/10.1111/jmg.12071

White, R. W., Powell, R., & Phillips, G. N. (2003). A mineral equilibria study of the hydrothermal alteration in mafic greenschist facies rocks at Kalgoorlie, Western Australia. *Journal of Metamorphic Geology*, *21*(5), 455–468. https://doi.org/10.1046/j.1525-1314.2003.00454.x

Wilkin, R. T., & Barnes, L. H. (1998). Solubility and stability of zeolites in aqueous solution: I. Analcime, Na-, and K-cIinoptilolite. *American Mineralogist*, *83*(7-8), 746–761. https://doi.org/10.2138/am-1998-7-807.

Wilkinson, J. F. G., & Hensel, H. D. (1991). An analcime mugearite-megacryst association from north-eastern New South Wales: Implications for high-pressure amphibole-dominated fractionation of alkaline magmas. *Contributions to Mineralogy and Petrology*, *109*(2), 240–251. https://doi.org/10.1007/BF00306482

Willner, A. P., Massonne, H.-J., Barr, S. M., & White, C. E. (2013). Very low- to low-grade metamorphic processes related to the collisional assembly of Avalonia in SE Cape Breton Island (Nova Scotia, Canada). *Journal of Petrology*, *54*(9), 1849–1874. https://doi.org/10.1093/petrology/egt033

Zipfel, J., Schröder, C., Jolliff, B. L., Gellert, R., Herkenhoff, K. E., Rieder, R., et al. (2011). Bounce rock—A shergottite-like basalt encountered at Meridiani Planum, Mars. *Meteoritics & Planetary Science*, *46*(1), 1–20. https://doi.org/10.1111/j.1945-5100.2010.01127.x

Zolotov, M. Y., & Mironenko, M. V. (2016). Chemical models for martian weathering profiles: Insights into formation of layered phyllosilicate and sulfate deposits. *Icarus*, *275*, 203–220. https://doi.org/10.1016/j.icarus.2016.04.011